Forest-atmosphere exchange of reactive nitrogen in a low polluted area – Part I: Measuring temporal dynamics

Pascal Wintjen[1], Frederik Schrader[1], Martijn Schaap[2,3], Burkhard Beudert[4], and Christian Brümmer[1]

[1]Thünen Institute of Climate-Smart Agriculture, Bundesallee 68, 38116, Braunschweig, Germany
[2]TNO, Climate Air and Sustainability, Utrecht, 3584 CB, The Netherlands
[3]Institute of Meteorology, Freie Universität Berlin, 12165 Berlin, Germany
[4]Bavarian Forest National Park, 94481, Grafenau, Germany

Correspondence: Pascal Wintjen (pascal.wintjen@thuenen.de)

Abstract. Understanding the biosphere-atmosphere exchange characteristics of nitrogen is essential for the parameterization of modern deposition routines. For investigating temporal dynamics and responses of reactive nitrogen compounds to micrometeorology and biophysical factors, long-term flux measurements are needed. In this study, we investigate the exchange patterns of total reactive nitrogen (ΣN_r) and determine annual dry deposition budgets based on measured data at a low-polluted mixed forest located in the Bavarian Forest National Park (NPBW), Germany. Flux measurements of ΣN_r were carried out with a Total Reactive Atmospheric Nitrogen Converter (TRANC) coupled to a chemiluminescence dectector (CLD) for 2.5 years.

The average ΣN_r concentration was 3.1 μg N m^{-3}. Denuder measurements with DELTA samplers and chemiluminescence measurements of nitrogen oxides (NO_x) have shown that NO_x has the highest contribution to ΣN_r ($\sim 51\%$), followed by ammonia (NH_3) ($\sim 21\%$), ammonium (NH_4^+) ($\sim 15\%$), nitrate NO_3^- ($\sim 7\%$), and nitric acid (HNO_3) ($\sim 6\%$). Only slight seasonal changes were found in the ΣN_r concentration level whereas a seasonal pattern was observed for NH_3 and NO_x. NH_3 showed highest contributions to ΣN_r in spring and summer, NO_x in autumn and winter.

We observed mostly deposition fluxes at the measurement site with median fluxes ranging from -15 to -5 ng N m^{-2} s^{-1} (negative fluxes indicate deposition). Median deposition velocities ranged from 0.2 to 0.5 cm s^{-1}. In general, highest deposition velocities were recorded during high incident radiation, in particular from May to September. Our results suggest that seasonal changes in concentrations of the ΣN_r compounds and radiation were most likely influencing the deposition velocity (v_d). We found that from May to September higher temperatures, lower relative humidity, dry leaf surfaces, and no precipitation increase v_d. The effective canopy resistance ($R_{c,eff}$) was slightly lower at low relative humidity and higher ΣN_r concentrations. Aerodynamic (R_a) and boundary-layer resistance (R_b) showed a negligible contribution to v_d in comparison to $R_{c,eff}$ highlighting the importance of the surface resistance to the uptake of ΣN_r. Presumably, stomatal uptake seemed to be most responsible for ΣN_r during those months.

During rain and in periods of lower radiation, v_d was significantly lower and sometimes even negative indicating emission phases of ΣN_r. In those times, $R_{c,eff}$ increased, and R_a and R_b were in same order of magnitude as $R_{c,eff}$, and thus atmospheric resistances seemed to be as important as the surface resistance for the ΣN_r exchange. In periods of lower radiation and rain, cuticular or soil processes appeared to be relevant for the ΣN_r exchange.

No significant influence of temperature, humidity, friction velocity, or precipitation on ΣN_r dry deposition sums were found with differences between deposition estimates being within their uncertainty ranges. We used the Mean-Diurnal-Variation (MDV) approach for filling gaps of up to five days. Remaining gaps were replaced by a monthly average of the specific half-hour value. From June 2016 to May 2017 and June 2017 to May 2018, we estimated dry deposition sums of 3.8 ± 0.8 kg N ha^{-1} and 4.1 ± 1.1 kg N ha^{-1}, respectively. Mean total wet depositions were 8.0 kg N ha^{-1} and 6.8 kg N ha^{-1} for the timeframes 2016/2017 and 2017/2018, respectively. Adding results from the wet deposition measurements to the measurement years, we determined 11.8 kg N ha^{-1} and 10.9 kg N ha^{-1} as total nitrogen deposition, respectively.

Our findings provide a better understanding of exchange dynamics at low-polluted, natural ecosystems, thereby providing opportunities for further development of deposition models.

1 Introduction

Reactive nitrogen (N_r) compounds are essential nutrients for plants. However, an intensive supply of nitrogen by fertilisation or atmospheric deposition is harmful for natural ecosystems and leads to a loss of biodiversity through soil acidification and eutrophication (Krupa, 2003; Galloway et al., 2003) and may also threaten human health by acting as precoursors for ozone (O_3) and PM2.5 (Erisman et al., 2013). Atmospheric nitrogen load increased significantly during the last century due to intensive crop production and livestock farming (Sutton et al., 2011; Flechard et al., 2011, 2013; Sutton et al., 2013) (mainly through ammonia) and fossil fuel combustion by traffic and industry (mainly through nitrogen dioxide and nitrogen oxide). The additional amount of N_r enhances biosphere-atmosphere exchange of N_r (Flechard et al., 2011), affects plant health (Sutton et al., 2011) and influences the carbon sequestration of ecosystems such as forests (Magnani et al., 2007; Högberg, 2007; Sutton et al., 2008; Flechard et al., 2020), although the impact of increasing nitrogen deposition on forests carbon sequestration is still under investigation.

For estimating the biosphere-atmosphere exchange of N_r compounds such as nitrogen monoxide (NO), nitrogen dioxide (NO_2), ammonia (NH_3), nitrous acid (HONO), nitric acid (HNO_3) and particulate ammonium nitrate (NH_4NO_3), the eddy-covariance (EC) approach has proven its applicability on various ecosystems. The sum of these compounds is called total reactive nitrogen (ΣN_r) throughout this manuscript. For evaluating fluxes of NO and NO_2 the EC technique has been tested in earlier studies (Delany et al., 1986; Eugster and Hesterberg, 1996; Civerolo and Dickerson, 1998; Li et al., 1997; Rummel et al., 2002; Horii et al., 2004; Stella et al., 2013; Min et al., 2014). In recent years, progress has been made in EC measurements of NH_3 (Famulari et al., 2004; Whitehead et al., 2008; Ferrara et al., 2012; Zöll et al., 2016; Moravek et al., 2019). First attempts in applying EC had been made on HNO_3, organic nitrogen molecules, nitrate (NO_3^-), and ammonium aerosols (NH_4^+) (Farmer et al., 2006; Nemitz et al., 2008; Farmer and Cohen, 2008; Farmer et al., 2011). Due to typically low concentrations, high reactivity, and water solubility, measuring fluxes of N_r compounds is still challenging since instruments need a low detection limit and a response time of < 1 s (Ammann et al., 2012). Thus, fast-response instruments for measuring N_r compounds like HNO_3 or NH_3 are equipped with a special inlet and short heated tubes to prevent interaction with tube walls (see Farmer et al., 2006; Zöll et al., 2016). However, these instruments need regular maintenance, have a high power consumption, and need a

climate controlled environment for a stable performance. Considering the high technical requirements of these instruments, measuring fluxes of HNO_3 or NH_3 with these instrument is still challenging.

The Total Reactive Atmospheric Nitrogen Converter (TRANC) (Marx et al., 2012) converts all above mentioned N_r compounds to NO. In combination with a fast-response chemiluminescence detector (CLD), the system allows measurements of ΣN_r with a high sampling frequency. Due to a low detection limit and a response time of about 0.3 s, the TRANC-CLD system can be used for flux calculation based on the eddy-covariance (EC) technique. The TRANC-CLD system has been shown to be suitable for EC measurements above a number of different ecosystems (see Ammann et al., 2012; Brümmer et al., 2013; Zöll et al., 2019; Wintjen et al., 2020).

Prior EC studies of ΣN_r or its compounds were carried out above managed field sites or close to agricultural or industrial emission hotspots, in order to focus on measuring the impact of environmental pollution or fertilization on (crop) plants. Only a few studies were conducted at remote locations, but were mainly focusing only on single N_r compounds (e.g., Wyers and Erisman, 1998; Horii et al., 2004, 2006; Wolff et al., 2010; Min et al., 2014; Geddes and Murphy, 2014; Hansen et al., 2015). At remote sites, concentrations of reactive N_r compounds are typically low and close to the detection limit of the deployed instruments. Zöll et al. (2019) demonstrated that the TRANC-CLD system is able to detect concentrations and fluctuations of ΣN_r accurately even at low ambient levels. It was the first study presenting short-term flux measurements of ΣN_r conducted with the same instrumentation at the measurement site with a focus on establishing a link between the drivers of both ΣN_r and CO_2. The authors identified incident radiation as primary driver for ΣN_r and CO_2 fluxes. Investigations on light response curves exhibited a reversal point for ΣN_r highlighting the existence of a canopy compensation point. The overall concentration of ΣN_r was identified as secondary driver for the ΣN_r exchange showing that processes affecting the physical and chemical properties of ΣN_r are more relevant than other micrometeorological drivers for the ΣN_r fluxes. Further analyses on deposition velocities and corresponding aerodynamic, boundary layer, and canopy resistances of ΣN_r allow to examine if the exchange is driven by turbulent or canopy processes. These investigations were formerly made for individual components of ΣN_r. For example, Wolff et al. (2010) found that aerosol fluxes of total ammonium and total nitrate were driven by aerodynamic processes. NH_3 features bidirectional exchange through stomata and cuticles (e.g., Farquhar et al., 1980; Sutton et al., 1995, 1998; Wyers and Erisman, 1998; Flechard et al., 1999; Milford et al., 2001; Nemitz et al., 2001; van Zanten et al., 2010; Wichink Kruit et al., 2010, 2017). NO_2 exhibits mainly stomatal and insignificant cuticular deposition (e.g., Rondon et al., 1993; Rondón and Granat, 1994; Thoene et al., 1991, 1996; Gessler et al., 2000, 2002; Sparks et al., 2001; Teklemmariam and Sparks, 2006; Chaparro-Suarez et al., 2011; Breuninger et al., 2013; Stella et al., 2013) whereas NO emissions are driven by soil microbial activities, which are influenced by soil temperature, soil moisture, and soil nitrogen (e.g., Remde et al., 1989; Remde and Conrad, 1993; Fowler et al., 1998; Ludwig et al., 2001; Schindlbacher et al., 2004; Behrendt et al., 2014; Medinets et al., 2016). Since N_r species exhibit an interannual variability and various reaction pathways, the exchange mechanisms of ΣN_r change through the seasons. With the availability of long-term flux measurements at a remote location, we were able to investigate seasonal changes in deposition velocities and resistances at low concentrations of ΣN_r and its components. An evaluation could be important for inferential deposition models in order to validate bidirectional resistance schemes.

During a measurement campaign instrumental performance issues and/or periods of insufficient turbulence arise, which require a quality flagging of processed fluxes. Afterwards, the resulting gaps in the measured time-series need to be filled in order to properly estimate long-term deposition budgets. Known gap-filling strategies include the Mean-Diurnal-Variation (MDV) method (Falge et al., 2001), look-up tables (LUT) (Falge et al., 2001), non-linear regression (NLR) (Falge et al., 2001), marginal distribution sampling (MDS) (Reichstein et al., 2005), and artificial neural networks (Moffat et al., 2007). However, most of these methods have in common that they were originally designed for carbon dioxide (CO_2) or other inert gases. MDS requires a short-term stability of fluxes and micrometeorological parameters. This condition is not necessarily fulfilled for ΣN_r and its components. Their exchange patterns are characterized by a higher variability for different time scales leading to a lower autocorrelation and non-stationarities in flux time series compared to inert gases like CO_2. It is, on the other hand, possible to use statistical methods like MDV or linear interpolation to fill short gaps in flux time series. This was done by Brümmer et al. (2013), but filling long gaps with this technique is not recommended. Since exchange patterns of ΣN_r can substantially vary each day depending on the composition of ΣN_r and micrometeorology, it is questionable if statistical methods are suitable for ΣN_r considering the high reactivity and chemical properties of its compounds.

The study presented here is the first one showing long-term flux measurements of ΣN_r above a remote forest focusing on the impact of environmental controls on fluxes, deposition velocities, and resistances. We discuss the observed flux pattern of ΣN_r (1), investigate the influence of micrometeorology on determined deposition velocities and (canopy) resistances (2), and show the influence of micrometeorological parameters on dry deposition sums estimated with the MDV approach (3). Wet deposition results obtained from bulk and wet-only sampler measurements are complementarily used to estimate total deposition.

Part II of the paper will present the usage of the acquired dataset in a modeling framework to estimate annual N budgets. Modeled fluxes and deposition velocities of the ΣN_r components will be compared to values reported in literature. Similar to Part I, the influence of micrometeorology on modeled fluxes, deposition velocities, and resistance will be investigated. Dry depositions estimated with the EC method will be compared to results from modeling approaches using in-situ and modeled input parameters and to canopy outflow measurements. We will discuss the ecological impact of nitrogen deposition on forest ecosystems. A comparison to annual N budgets reported for other forest ecosystems will be carried out.

2 Materials and Methods

2.1 Site and meteorological conditions

Measurements were made in the Bavarian Forest National Park (NPBW) (48°56'N 13°25'E, 807 m a.s.l) in southeast Germany. The unmanaged site is located in the Forellenbach catchment ($\sim 0.69\,km^2$ (Beudert and Breit, 2010)), is surrounded by a natural, mixed forest, and is about 3 km away from the Czech border. Due to the absence of emission sources of N_r in the surroundings of the measurement site, mean annual concentrations of NO_2 (2.1-4.8 ppb), NO (0.4-1.6 ppb) and NH_3 (1.4 ppb) are low (Beudert and Breit, 2010). The site is characterized by low annual temperatures (6.1°C) and high annual precipitation (1327 mm) measured at 945 m a.s.l. Annual temperature in 2016, 2017, and 2018 was 6.8°C, 6.9°C, and 8.0°C and precipitation was 1208 mm, 1345 mm, and 1114 mm, respectively. There are no industries or power plants nearby, only small villages with

moderate animal housing and farming (Beudert et al., 2018). Due to these site characteristics, measurements of the ΣN_r background deposition are possible. For monitoring air quality and micrometeorology a 50 m tower was installed in the 1980s. Measurements of ozone, sulphur dioxide, and NO_x, the sum of NO and NO_2, have been conducted since 1990 (Beudert and Breit, 2010). The Forellenbach site is part of the International Cooperative Program on Integrated Monitoring of Air pollution Effects on Ecosystems (ICP IM) within the framework of the Geneva Convention on Long-Range Transboundary Air Pollution (UNECE, 2020) and belongs to the Long Term Ecological Research (LTER) network (LTER, 2020). The Federal Environment Agency (UBA) and NPBW Administration have been carrying out this monitoring program in the Forellenbach catchment. The flux footprint consists of Norway spruce (*Picea abies*) and European beech (*Fagus sylvatica*) covering approximately 80% and 20% of the footprint, respectively (Zöll et al., 2019). During the study period, maximum stand height was less than 20 m since dominating Norway spruce are recovering from a complete dieback by bark beetle in the mid-1990s and 2000s (Beudert and Breit, 2014).

2.2 Experimental setup

Flux measurements of ΣN_r were made from January 2016 until end of June 2018 at a height of 30 m above ground. A custom-built ΣN_r converter (total reactive atmospheric nitrogen converter, TRANC) after Marx et al. (2012) and a 3-D ultrasonic anemometer (GILL-R3, Gill Instruments, Lymington, UK) were attached on different booms close to each other at 30 m height. The TRANC was connected via a 45 m opaque PTFE tube to a fast-response chemiluminescence detector (CLD 780 TR, ECO PHYSICS AG, Dürnten, Switzerland), which was housed in an air-conditioned box at the bottom of the tower. The CLD was coupled to a dry vacuum scroll pump (BOC Edwards XDS10, Sussex, UK), which was placed at ground level, too. The inlet of the TRANC is designed after Marx et al. (2012) and Ammann et al. (2012). The conversion of ΣN_r to NO is split in two steps. Firstly, a thermal conversion occurs in an iron-nickel-chrome tube at 870°C. The thermal conversion of NH_4NO_3 leads to gaseous NH_3 and HNO_3. The latter is split up into to NO_2, H_2O, and O_2. NH_3 oxidized by O_2 at a platinum gauze to NO. HONO is split up to NO and a hydroxyl radical (OH). In a second step, a gold tube passively heated to 300°C catalytically converts the remaining oxidized N_r species to NO. In this process, carbon monoxide (CO) is acting as a reducing agent. More details about the chemical conversion steps can be found in Marx et al. (2012). A critical orifice was mounted at the TRANC's outlet and restricted the mass flow to 2.1 $\mathrm{L\,min^{-1}}$ after the critical orifice assuring low pressure along the tube. The mass flow rate before the critical orifice was the same as after the critical orifice. Since mass flow was equal to both sides of the critical orifice, a difference in flow velocity was induced due to the reduction in pressure. Flow velocities were not measured for the different sections.

The conversion efficiency of the TRANC had been investigated by Marx et al. (2012). They found 99% for NO_2, 95% for NH_3, and 97% for a gas mixture of NO_2 and NH_3. Conversion efficiencies for sodium nitrate ($NaNO_3$), ammonium nitrate (NH_4NO_3), and ammonium sulfate ($(NH_4)_2SO_4$) were 78%, 142%, and 91%, respectively. Overall, the results indicate that the TRANC is able to convert aerosols and gases efficiently to NO. For further details we refer to the publication of Marx et al. (2012).

For determining local turbulence - wind speed, wind direction, friction velocity (u_*) - measurements of the wind components (u, v, and w) were conducted using the sonic anemometer. Close to the sonic, an open-path LI-7500 infrared gas analyzer (IRGA) for measuring CO_2 and H_2O concentrations was installed.

For investigating the local meteorology, air temperature and relative humidity sensors (HC2S3, Campbell Scientific, Logan, Utah, USA) were mounted at four different heights (10, 20, 40, and 50 m above ground). At the same levels, wind propeller anemometers (R.M. Young, Wind Monitor Model 05103VM-45, Traverse City, Michigan, USA) were mounted on booms. Leaf wetness sensors designed after the shape of a leaf (Decagon, LWS, n=6, Pullman, Washington, USA) were attached to branches of a spruce and a beech tree near the tower. Sensors of the beech tree were at heights of approximately 2.1 m, 5.6 m, and 6.1 m, sensors of the spruce tree were at heights of 2.1 m, 4.6 m, and 6.9 m. These measurements started in April 2016. Due to a wetting of the sensor's surface, the electric conductivity of the material changes. This signal, the leaf wetness, was converted by the instrument to dimensionless counts. Based on the number and range of counts, different wetness states could be defined. Half-hourly leaf wetness values were in the range from 0 to 270. In this study, we defined the wetness states "dry" and "wet". The condition wet can be induced by the accumulation of hygroscopic particles extending the duration of the wetness state or water droplets. In order to classify a leaf as dry or wet, we determined a threshold value based on the medians of leaf wetness values. During daylight (global radiation $> 20\,\mathrm{W\,m^{-2}}$), medians ranged from 1.1 to 2.0 and were between 4.1 and 9.4 during nighttime. During nighttime, medians are higher due to dew formation. According to the values determined during daylight, we set the threshold value to 1.5 for all sensors. If the leave wetness value was lower than 1.5, the leaf was considered as dry. Otherwise, the leaf surface was considered as wet. To take differences between the sensors into account, all sensors were used to derive a common wetness Boolean. Therefore, the number of dry sensors were counted for each half-hour: If at least three sensors were considered as dry, the corresponding half-hour was considered as mostly dry. A cleaning of sensors was not conducted because contamination effects could be corrected by implemented algorithms. The derived wetness Boolean was used in the analysis of deposition velocities and resistances (Sec. 3.2).

Ambient NH_3 was collected by passive samplers at ground level (1.5), 10, 20, 30, and 50 m from January 2016 to June 2018. Measurements at 40 m started in July 2016. The collector at ground level was moved to 40 m. Passive samplers of the IVL type (Ferm, 1991) were used for NH_3, and the exposition duration was approximately one month at a time. DELTA measurements (DEnuder for Long-Term Atmospheric sampling (e.g., Sutton et al., 2001; Tang et al., 2009)) of NH_3, HNO_3, SO_2, NO_3^-, and NH_4^+ were taken at the 30-m platform. The DELTA measurements had the same sampling duration as the passive samplers. The denuder preparation and subsequent analyzing of the samples was identical to the procedure for KAPS denuders (Kananaskis Atmospheric Pollutant Sampler, (Peake, 1985; Peake and Legge, 1987)) given in Dämmgen et al. (2010) and Hurkuck et al. (2014). We controlled the pump to keep flow at a constant level and checked the pipes for contamination effects before analyzing. Blank values were used as additional quality control.

Fast-response measurements of NH_3 were performed with a NH_3 Quantum Cascade Laser (QCL) (model mini QC-TILDAS-76 from Aerodyne Research, Inc. (ARI, Billerica, MA, USA)) at 30 m height, too. The setup of the QCL was the same as described in Zöll et al. (2016). Further details about the location and specifications of the installed instruments can be found in Zöll et al. (2019) and Wintjen et al. (2020).

At the top of the tower (50-m platform), measurements of NO and NO_2 were conducted by the NPBW using a chemiluminescence detector (APNA - 360, HORIBA, Tokyo, Japan). Measurements of global radiation and atmospheric pressure were also conducted at 50 m. Precipitation was measured at a location in 1 km southwest distance from the tower according to WMO (World Meteorological Organization) guidelines (Jarraud, 2008), and data were quality-checked by the NPBW (Beudert and Breit, 2008, 2010). Wet deposition was collected as bulk and wet-only samples in weekly intervals in close vicinity to the tower using four samplers, three bulk samplers and one wet-only sampler, at an open site.

2.3 Flux calculation and post processing

The software package EddyMeas, included in EddySoft (Kolle and Rebmann, 2007), was used to record the data with a time resolution of 10 Hz. Analog signals from CLD, LI-7500, and the sonic anemometer were collected at the interface of the anemometer and joined to a common data stream. Flux determination covered the period from 1 January 2016 to 30 June 2018. Half-hourly fluxes were calculated by the software EddyPro 7.0.4 (LI-COR Biosciences, 2019). For flux calculation a 2-D coordinate rotation of the wind vector was selected (Wilczak et al., 2001), spikes were detected and removed from time series after Vickers and Mahrt (1997), and block averaging was applied. Due to the distance the from inlet of TRANC to the CLD, a time lag between concentration and sonic data was inevitable. The covariance maximization method allows to estimate the time lag via shifting the time series of vertical wind and concentration against each other until the covariance is maximized (Aubinet et al., 2012; Burba, 2013). The time lag was found to be approximately 20 s (see Fig. S1). Figures with the notation Sn where n=1...9 can be found in the supplemental material. We instructed EddyPro to compute the time lag after covariance maximization with default setting while using 20 s as default value and set the range from 15 s to 25 s (for details see Wintjen et al., 2020). For correcting flux losses in the high-frequency range we used an empirical method suggested by Wintjen et al. (2020), which uses measured cospectra of sensible heat ($\mathrm{Co}(w,T)$) and $\Sigma\mathrm{N_r}$ flux ($\mathrm{Co}(w,\Sigma\mathrm{N_r})$) and an empirical transfer function. We followed their findings and used bimonthly medians of the damping factors for correcting calculated fluxes since the chemical composition of $\Sigma\mathrm{N_r}$ exhibits seasonal differences (see Fig. 4 and Brümmer et al., 2013). On average, the damping factor was 0.78, which corresponds to flux loss of 22% (Wintjen et al., 2020). The authors determined flux loss factors for two different ecosystems, which are different, for example, in the composition of $\Sigma\mathrm{N_r}$. They assumed that the differences in flux losses are also related to the chemical composition of $\Sigma\mathrm{N_r}$. The low-frequency flux loss correction was done with the method of Moncrieff et al. (2004), and the random flux error was calculated after Finkelstein and Sims (2001).

Previous measurements with the same CLD model by Ammann et al. (2012) and Brümmer et al. (2013) revealed that the device is affected by ambient water vapour due to quantum mechanical quenching. Excited NO_2 molecules can reach ground state without emitting a photon by colliding with a H_2O molecule, thereby no photon is detected by the photo cell. It results in a sensitivity reduction of 0.19% per $1\,\mathrm{mmol\,mol^{-1}}$ water vapour increase. Thus, calculated fluxes were corrected after the approach by Ammann et al. (2012) and Brümmer et al. (2013) using the following equation:

$$F_{\mathrm{NO,int}} = -0.0019 \cdot c_{\Sigma\mathrm{N_r}} \cdot F_{\mathrm{H_2O}} \tag{1}$$

The NO interference flux $F_{\mathrm{NO,int}}$ has to be added to every estimated flux value. $c_{\Sigma \mathrm{N_r}}$ is the measured concentration of the CLD and $F_{\mathrm{H_2O}}$ the estimated H_2O flux from the LI-7500 eddy-covariance system. The correction contributed approximately 132 g N ha^{-1} to two years of TRANC flux measurements if the Mean-Diurnal-Variation (MDV) approach was used as gap-filling approach. Half-hourly interference fluxes were between -3 and +0.3 ng N m^{-2} s^{-1}. Their random flux uncertainty ranged between 0.0 and 0.5 ng N m^{-2} s^{-1}.

After flux calculation, we applied different criteria to identify low-quality fluxes. We removed fluxes, which were outside the range of -520 ng N m^{-2} s^{-1} to 420 ng N m^{-2} s^{-1}, discarded periods with insufficient turbulence ($u_* < 0.1$ m s^{-1}) (see Zöll et al., 2019), and fluxes with a quality flag of "2" (Mauder and Foken, 2006). These criteria ensure the quality of the fluxes, but lead to systematic data gaps in flux time series. Instrumental performance problems led to further gaps in the time series. Most of them were related to maintaining and repairing of the TRANC and/or CLD, for example, heating and pump issues, broken tubes, empty O_2 gas tanks (O_2 is required for CLD operation), power failure, or a reduced sensitivity of the CLD. The reduction in sensitivity may be caused by reduced pump performance leading to an increase in sample cell pressure. If pressure in the sampling cell is outside the regular operating range, low pressure conditions needed for the detection of photons emitted by excited NO_2 molecules may not hold. Pump efficiency was controlled at least monthly, and tip seals were replaced if necessary. The sensitivity of the CLD could also be reduced by changes in the O_2 supply from gas tanks to ambient, dried box air if O_2 gas tanks were empty. Issues in the air-conditioning system of the box could also affect the sensitivity of the CLD. An influence of aging on the inlet, tubes, and filters may also affect the measurements. In order to minimize an impact on the measurements, half-hourly raw concentrations were carefully checked for irregularities like spikes or drop-outs by visual screening. Considering the time period of ongoing measurements from the beginning of January 2016 till June 2018, the quality flagging resulted in 52.2% missing data. The loss in flux data is higher than values reported by Brümmer et al. (2013). They reported a flux loss of 24% caused by u_* filtering. In this study, the same u_* threshold caused a flux loss of approximately 15.5%. 32.7% data loss from January 2016 to June 2018 was caused by instrumental performance problems showing that TRANC-CLD system was overall operating moderately stable. For gap-filling we applied the MDV approach to gaps in the $\Sigma \mathrm{N_r}$ flux time series. The window for filling each gap was set to $\pm$5 days. Remaining, long-term gaps were filled by a monthly average of the specific half-hour value estimated from non-gap-filled fluxes (Fig. 6) in order to estimate $\Sigma \mathrm{N_r}$ dry deposition sums from June 2016 to May 2017 and from June 2017 to May 2018. Uncertainties of the gap-filled fluxes are estimated by the standard error of the mean.

As outlined in Sec. 2.2, measurements of NH_3 were made with a QCL at high temporal resolution. In combination with the sonic anemometer, it gives the opportunity to determine NH_3 fluxes and to further investigate the non-NH_3 component of the $\Sigma \mathrm{N_r}$ flux. However, a calculation of the NH_3 fluxes with the EC method was not possible in this study. No consistent NH_3 time lag was found making flux evaluation impossible. Due to regular pump maintenance, cleaning of the inlet and absorption cell, issues related to the setup of the QCL were unlikely to be the cause. We suppose that the variability in the measured NH_3 concentrations was not sufficiently detectable by the instrument. Significant short-term variability in the $\Sigma \mathrm{N_r}$ raw concentrations were not found in the NH_3 signal even in spring or summer. Thus, no robust time lag estimation could be applied to the vertical wind component of the sonic anemometer and the NH_3 concentration. Recently, Ferrara et al. (2021)

found large uncertainties for low NH_3 fluxes measured with the same QCL model. Cross-covariance functions had a low signal-to noise ratio indicating that most of the fluxes were close to the detection limit.

2.4 Determining deposition velocity and canopy resistance of ΣN_r from measurements

In surface-atmosphere exchange models of N_r species like NO_2, NO, NH_3, HNO_3, or nitrogen aerosols, the flux (F_t) is calculated by multiplying concentrations of a trace gas modeled or measured at a reference height ($\chi_a(z-d)$) with a so-called deposition velocity ($v_d(z-d)$) where z is measurement height and d the zero-plane displacement height (van Zanten et al., 2010). The deposition velocity can be described by an electrical analogy and is defined as the inverse of the sum of three resistances (Wesely, 1989; Erisman and Wyers, 1993). According to its definition a positive v_d indicates deposition, a negative v_d emission. Note that, strictly speaking, for bidirectional exchange v_d needs to be interpreted as an "exchange velocity", i.e. it can technically become negative during emission phases. Equations are the same as for v_d (van Zanten et al., 2010).

$$F_t = -v_d(z-d) \cdot \chi_a(z-d) \quad \text{with } v_d = (R_a(z-d) + R_b + R_{c,\text{eff}})^{-1} \tag{2}$$

R_a is the aerodynamic resistance, R_b is the quasi-laminar boundary layer resistance, and $R_{c,\text{eff}}$ is the (effective) canopy resistance (i.e., including the effects of compensation points for some species). R_a is adapted from Garland (1977) and R_b based on Jensen and Hummelshøj (1995, 1997). They are influenced by micrometeorological parameters, surface conditions, and chemical properties of the N_r species of interest. R_a is defined as

$$R_a(z-d) = \frac{u(z-d)}{u_*^2} - \frac{\Psi_H(\frac{z-d}{L}) - \Psi_M(\frac{z-d}{L})}{u_* \cdot \kappa} \tag{3}$$

where u_* is the friction velocity, $u(z-d)$ is the wind speed at the reference height, κ is the von Kàrmàn Constant (≈ 0.41), L is the Obukhov length, and Ψ_H and Ψ_M are the integrated stability corrections for entrained scalars and momentum following Webb (1970) and Paulson (1970), respectively. R_b is given as

$$R_b = \frac{\nu_{air}}{D_{cp}} \cdot \left(\frac{c}{LAI^2} \cdot \frac{l \cdot u_*}{\nu_{air}} \right)^{\frac{1}{3}} \cdot \frac{1}{u_*} \tag{4}$$

where ν_{air} is the kinematic viscosity of air, D_{cp} is the molecular diffusivity of the N_r species, LAI is the leaf area index, c an empirically determined constant, which is set to 100 according to Jensen and Hummelshøj (1997), and l represents a typical leaf width (Jensen and Hummelshøj, 1995), which is set to 0.01 m. We determined the molecular diffusion coefficient for ΣN_r as the weighted average of the campaign-wise averages of HNO_3, NH_3, NO, and NO_2 multiplied with their individual molecular diffusivities adapted from Massman (1998) and Durham and Stockburger (1986). It should be noted that particles are mostly not affected by a boundary-layer resistance compared to gases. However, the analysis of DELTA measurements showed that the mean particle contribution to the ΣN_r concentrations is only 22%. LAI was estimated after the same scheme used for the depostion module DEPAC (DEPosition of Acidifying Components) (Erisman et al., 1994) (see Appendix B of van Zanten et al., 2010). A linear increase of the LAI was calculated from mid of April to begin of May, a linear decrease from October to begin of November. Values ranged between 4.1 and 4.8. Fig. 1 shows the LAI for measured fractions of spruce and beech forest.

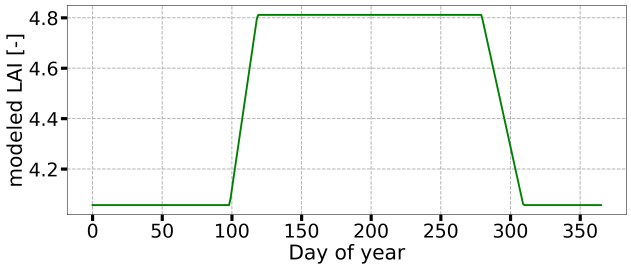

Figure 1. LAI following van Zanten et al. (2010) for measured fractions of coniferous forest (81.1%) and deciduous forest (18.9%) within the flux foot print for a year.

Considering only R_a and R_b, the maximum deposition velocity permitted by micrometeorological conditions is

$$v_{\mathrm{d,max}}(z-d) = (R_\mathrm{a}(z-d) + R_\mathrm{b})^{-1} \tag{5}$$

Subtracting $v_{\mathrm{d,max}}(z-d)$ from measured $v_\mathrm{d}(z-d)$, allows to determine an effective canopy resistance ($R_{\mathrm{c,eff}}$) for $\Sigma \mathrm{N_r}$

$$R_{\mathrm{c,eff}} = \frac{1}{v_\mathrm{d}(z-d)} - \frac{1}{v_{\mathrm{d,max}}(z-d)} \tag{6}$$

Commonly, $R_{\mathrm{c,eff}}$ consists of different resistances contributing to the uptake capacity of the surface, e.g., a stomatal resistance (R_stom), a cuticular resistance (R_w), and a soil resistance (R_soil). R_stom and R_w describe the exchange through the stomata of plants and with wet leaf surfaces, respectively. Interactions with the soil are merged in R_soil.

For $\mathrm{N_r}$ species exhibiting a bidirectional exchange pattern like NH_3 (e.g., Farquhar et al., 1980; Sutton et al., 1995, 1998; Wyers and Erisman, 1998; Flechard et al., 1999; Milford et al., 2001; Nemitz et al., 2001; van Zanten et al., 2010; Wichink Kruit et al., 2010, 2017) the existence of a compensation point is assumed. In case of NH_3, the stomatal compensation point is the concentration, at which the gaseous ammonia concentration is in equilibrium with dissolved ammonia in the apoplastic fluid at the reference height. In equilibrium state, the stomatal flux is zero (Farquhar et al., 1980; Sutton et al., 1994, 1998; Nemitz et al., 2000). Consequently, as long as the stomatal concentration is lower than the ambient concentration an uptake of $\mathrm{N_r}$ species happens. The cuticular exchange is also bidirectional for NH_3 (Wentworth et al., 2016). Observations by Neirynck and Ceulemans (2008) indicated the existence of a cuticular compensation point (Nemitz et al., 2001; Massad et al., 2010; Wichink Kruit et al., 2010; Schrader et al., 2016; Wichink Kruit et al., 2017), at which the gaseous NH_3 concentration is in equilibrium with the solution on the external leaf surfaces.

Hints on NO_2 compensation points were found, for example by Thoene et al. (1996). Breuninger et al. (2013) detected compensation points for NO_2 but compensation point concentrations were not significant. However, the authors found a large uncertainty showing that the determination of compensation points for NO_2 is challenging (Chaparro-Suarez et al., 2011; Breuninger et al., 2013; Delaria et al., 2018, 2020).

No clear evidence is found on compensation points for HNO_3. The assumption of an ideal uptake seems to be questionable (Tarnay et al., 2002). Farmer and Cohen (2008) detected significant emission fluxes of HNO_3 during summer above a spruce forest. HNO_3 emission during summer can be caused by evaporation of NH_4NO_3, which is favored at temperatures above 20°C

(Wyers and Duyzer, 1997; Van Oss et al., 1998). The mechanism explaining the HNO_3 emission is still under investigation (Nemitz et al., 2004).

Nitrogen aerosols are likely deposited, and their flux pattern is driven by R_a (Wolff et al., 2010). Soil microbial activities imply a compensation point for soil NO fluxes, which depends on soil temperature, soil water content and N availability (Fowler et al., 1998; Behrendt et al., 2014).

For the evaluation of v_d and corresponding resistances shown in Sec. 3.2, Eq. (2) to (6) were used.

3 Results

3.1 Concentrations, deposition velocities, and fluxes of ΣN_r during the measurement campaign

Figure 2 shows ambient concentrations of ΣN_r (black), NH_3 (red) and NO_x (blue) as half-hourly averages for the entire measurement campaign. Data gaps were mostly related to instrumental performance problems. No ΣN_r measurements were possible until end of May 2016 due to heating problems of the TRANC.

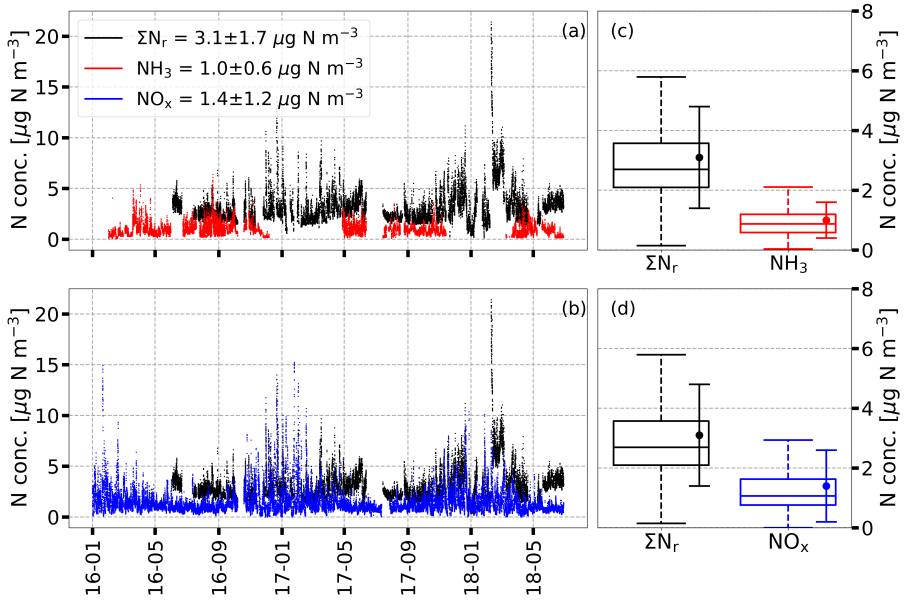

Figure 2. Half-hourly averaged concentrations of ΣN_r (black), NH_3 (red) and NO_x (blue) in μg N m^{-3} from 1 January 2016 to 30 June 2018 displayed in (a) and (b). Box plots (box frame = 25 % to 75 % interquartile range (IQR), bold line = median, whisker = 1.5· IQR) with average values (dots) shown in (c) and (d). Error bars represent one standard deviation.

ΣN_r concentrations exhibited highest values during the winter months. For example, values were higher than 10 μg N m^{-3} during January 2017 and February 2018. NO_x showed a relatively high concentration level during winter, too. During spring and summer, NO_x values were mostly lower than 2 μg N m^{-3} and hence, their contribution to ΣN_r decreased. However, ΣN_r

values remained around 3 μg N m^{-3} and reached values up to 6 μg N m^{-3}, which was related to higher NH_3 concentrations during these periods. ΣN_r concentration was 3.1 μg N m^{-3} on average, NH_3 was 1.0 μg N m^{-3}, and NO_x was 1.4 μg N m^{-3} on average with the latter values being in agreement with concentrations reported by Beudert and Breit (2010). Averaged NH_3 concentrations of the QCL agreed well with NH_3 from passive samplers and DELTA measurements (Fig. S2). Overall, the agreement in the annual pattern was good, but a bias between the QCL and the diffusion samplers was found. From passive sampler measurements, an increase in the NH_3 concentration with measurement height could be observed. At 10 m (in the canopy), the lowest NH_3 concentrations were measured. No systematic difference was found between 20 m and 30 m. At 50 m, NH_3 was slightly higher (0.1 μg N m^{-3}) than 30 m. During winter, the difference in measurement heights diminished. Slightly higher NH_3 concentration were observed at 10 m in winter.

The observations made for the seasonal changes of the half-hourly ΣN_r concentrations are also visible for their monthly medians (Fig. S3). Figure S3 shows monthly box plots of the concentrations. In general, median concentrations were almost similar for the entire campaign with slight differences between the years. Medians were between 2 and 3.5 μg N m^{-3}. From July to September, concentrations were slightly higher in 2016 than in 2017. During this period, IQRs and whiskers were the smallest for the entire year showing less variability in ΣN_r concentrations. In spring and winter, median concentrations were higher, and concentrations covered a wider range compared to the summer month. Figure S4 shows the corresponding diurnal patterns for each month. During the day, ΣN_r concentrations were almost stable. Averaged values showed variations of less than 1 μg N m^{-3}. If concentrations were averaged for each season (not shown), slightly higher concentrations were observed from 9:00 to 15:00 LT and lower values during the night.

Figure 3 shows absolute concentrations of individually measured N_r compounds as stacked bars and ΣN_r from the TRANC from January 2016 to June 2018. TRANC and NO_x measurements were averaged to exposition periods of DELTA measurements. DELTA measurements recorded at an insufficient pump flow were excluded from the analysis. Missing NH_3 values in the DELTA time series were filled by NH_3 data determined from the passive sampler mounted at 30 m. Remaining data gaps in the DELTA time series of NH_3, HNO_3, NH_4^+, and NO_3^- were replaced by monthly averages from other years. The procedure was not applied to the time period covering February 2018 due to the unusually high ΣN_r concentrations.

The comparison of the TRANC with DELTA+NO_x revealed slight overestimations by the latter from August 2016 to October 2016 and from January to March 2017. On average, an underestimation by DELTA+NO_x of approximately 0.3 μg N m^{-3} with a standard deviation of 0.7 μg N m^{-3} was observed. The median value was about 0.35 μg N m^{-3}.

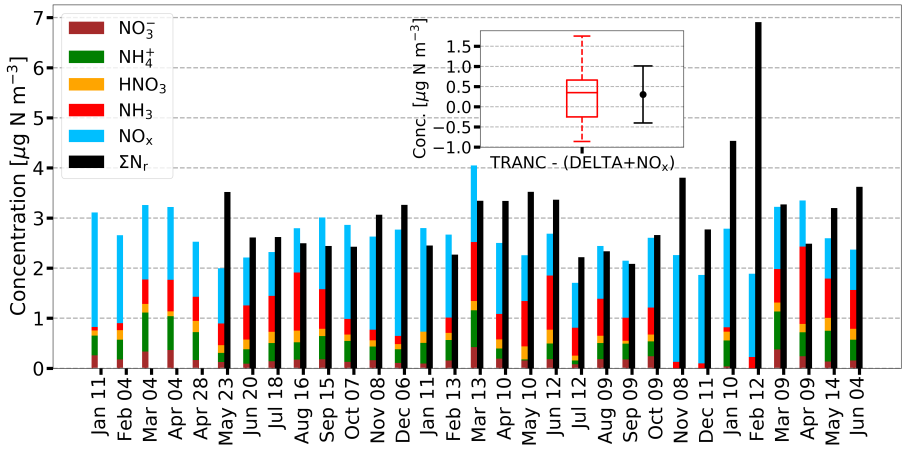

Figure 3. Monthly stacked concentration of TRANC, DELTA, and NO_x in μg N m^{-3} for the entire measurement campaign. Missing NH_3 measurements from the DELTA measurements caused by a low pump flow were filled with passive sampler values from 30 m. Replacing was done for December 2016 and 2017, January 2017, November 2017, and from February to April 2018. Gaps in the time series of the individual components were replaced by monthly averages estimated from other years if possible. NO_x and ΣN_r were averaged to the exposition periods of the DELTA samplers.

HNO_3, NH_4^+, and NO_3^- concentrations were nearly equal through the entire measurement campaign. Seasonal differences existed mainly for NH_3 and NO_x. We measured average concentrations of 0.56, 0.17, 0.40, 0.19, and 1.40 μg N m^{-3} for NH_3, HNO_3, NH_4^+, NO_3^-, and NO_x for the entire campaign, respectively. On average, the relative contribution of NH_3, HNO_3, NH_4^+, and NO_3^- to ΣN_r was less than 50% for the entire measurement campaign as visualized by Fig. 4. We further observed a low particle contribution to the ΣN_r concentrations ($\sim$ 22% on average) showing that the ΣN_r concentration pattern was mainly influenced by gaseous N_r compounds.

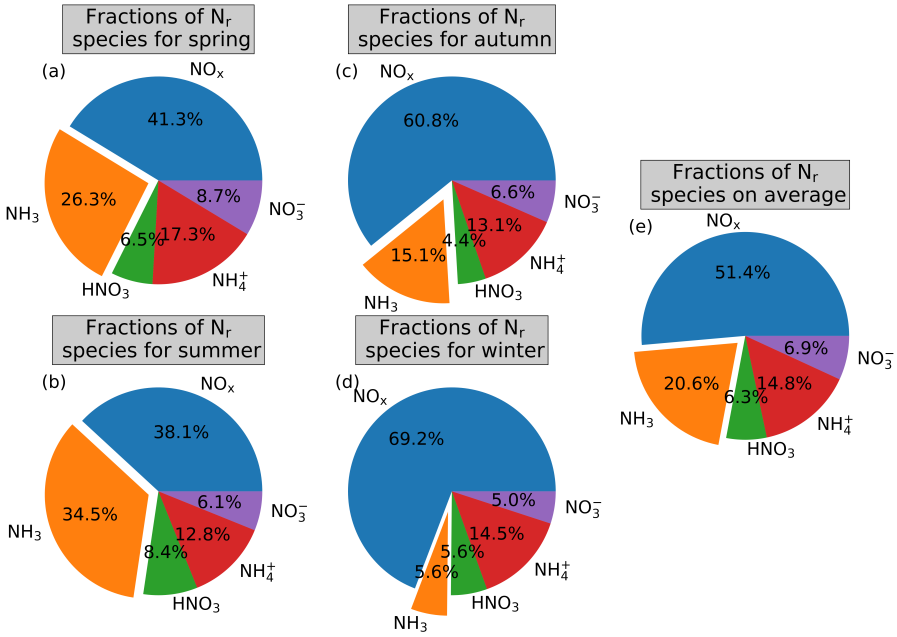

Figure 4. Pie charts showing the relative contribution of concentrations for NO_x, NH_3, NO_3^-, NH_4^+, and HNO_3 to ΣN_r based on DELTA samplers and NO_x measurements for different seasons of the year. NO_x measurements are averaged to exposition periods of the DELTA samplers. (a) to (d) refer to spring, summer, autumn, and winter, respectively. (e) shows the average relative contribution to ΣN_r for the entire measurement period.

In general, NO_x showed the highest contribution to ΣN_r and followed seasonal changes with highest values during winter and lowest values in summer. NH_3 showed also seasonal changes with concentrations lowest in winter and highest values in spring and summer. The contribution of HNO_3 was almost stable. A slight increase in the contribution was found for summer. As reported by Tang et al. (2020), HONO sticks to carbonate coated denuder surfaces, which are designed for collecting HNO_3. Thus, HNO_3 concentrations may be biased. NO_3^- and NH_4^+ exhibited slightly higher values for spring. Only small seasonal changes in the overall ΣN_r concentration were observed. As seen by Fig.3, ΣN_r concentrations were mostly between 2 and 4 μg N m^{-3}. We measured 3.3, 2.6, 2.5, and 3 μg N m^{-3} with the TRANC system for spring, summer, autumn, and winter, respectively.

Figure 5 shows the non-gapfilled ΣN_r fluxes depicted as box plots on monthly time scale. The convention is as follows: negative fluxes represent deposition, positive fluxes emission.

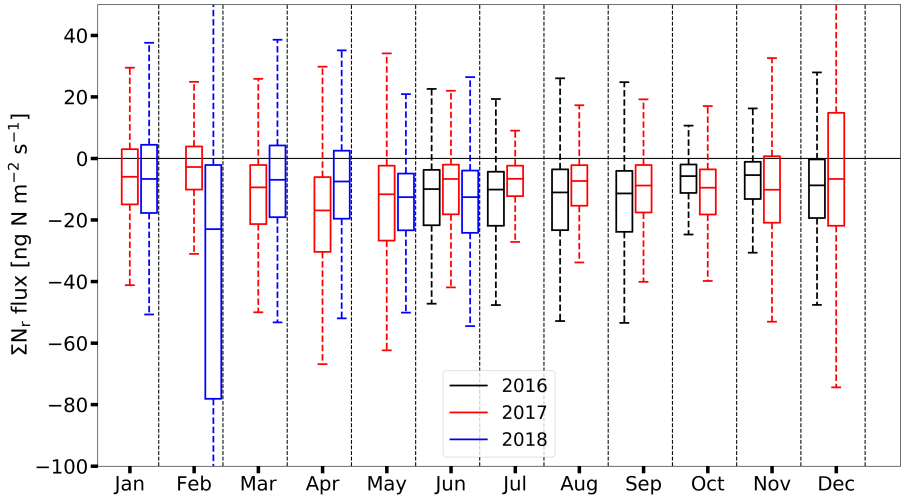

Figure 5. Time series of measured high-quality (flags "0" and "1") ΣN_r fluxes depicted as box plots on monthly basis (box frame = 25% to 75% interquartile ranges (IQR), bold line = median, whisker = 1.5· IQR) in ng N m^{-2} s^{-1}. Colors indicate different years. The displayed range was restricted from -100 to 50 ng N m^{-2} s^{-1}.

Almost all ΣN_r flux medians were between -15 and -5 ng N m^{-2} s^{-1} indicating that mainly deposition of ΣN_r occurred at our measurement site. Quality assured half-hourly fluxes showed 80% deposition and 20% emission fluxes. On half-hourly basis, fluxes were in the range from -516 to 399 ng N m^{-2} s^{-1}. The mean random flux error of the non-gapfilled, half-hourly fluxes was 5.9 ng N m^{-2} s^{-1} after Finkelstein and Sims (2001). The flux detection limit was calculated by multiplying 1.96 with the flux error (95% confidence limit) (see Langford et al., 2015). The latter was 11.5 ng N m^{-2} s^{-1}. Both values refer to the entire measurement campaign. Similar values were found by Zöll et al. (2019) at the same site covering a shorter period. In total, 51% of the non gap-filled fluxes were higher than the flux detection limit. It shows that for large parts nitrogen dry deposition was close to detection limit of the used measuring device and that nitrogen exchange happened at a comparatively low level.

In general, median deposition was almost on the same level for the entire campaign with slight seasonal differences. For instance, median deposition was slightly higher during spring and summer than during winter for 2016. However, median deposition during winter 2017 was similar to median deposition in summer 2017. Median deposition was significantly stronger from June 2016 till September 2016 than for the same period in 2017. IQR and whisker covered a wider range, too. The pattern changed for the time period from October to December. In December 2017, the IQR expanded in the positive range indicating emission events for a significant time period. The largest median deposition with 25 ng N m^{-2} s^{-1} and the widest range in IQR reaching approximately -80 ng N m^{-2} s^{-1} were registered in February 2018 indicating strong deposition phases during that month with sporadic emission events. Such phenomenons were not observed in the years before. In the following month, the deposition was slightly higher from March to April 2017 than for the same period in 2018. Fig. 6 shows averaged daily cycles for every month.

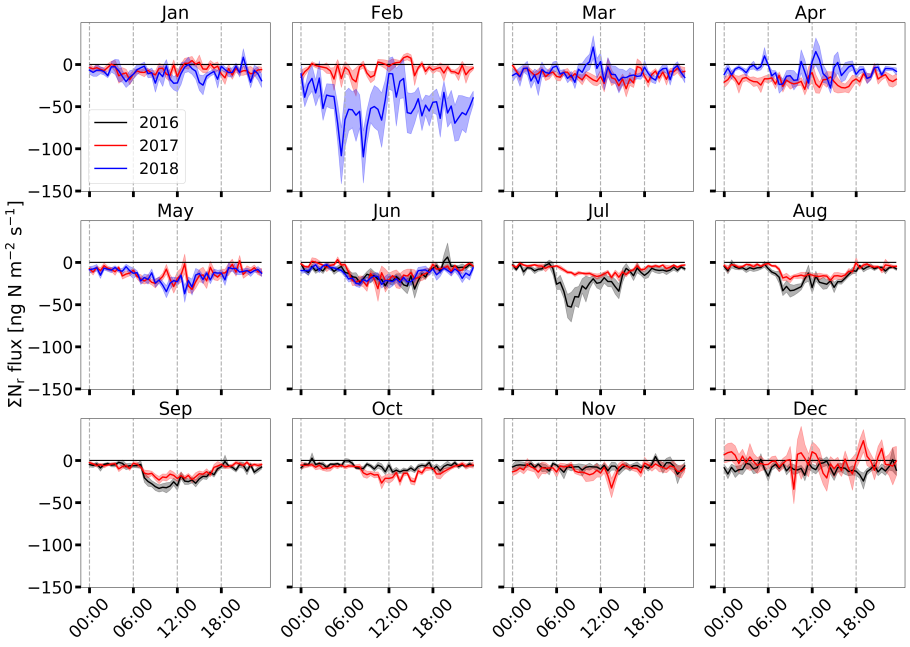

Figure 6. Mean daily cycle for every month of ΣN_r fluxes from June 2016 to June 2018 on half-hourly basis. The shaded area represents the standard error of the mean. Colors indicate different years.

In general, the ΣN_r daily cycle exhibited low deposition or neutral exchange during nighttime/evening and increasing deposition during daytime. Deposition rates were similar during the night for the entire campaign except for February 2018. Maximum deposition was reached between 9:00 and 15:00 LT. Deposition is enhanced from May until September showing fluxes between -40 and -20 ng N m^{-2} s^{-1}. From October to November and from December to February, the daily cycle weakened with almost neutral or slightly negative fluxes, mostly lower than -10 ng N m^{-2} s^{-1}. The daily cycles of the respective same months were mainly similar. However, during certain months, which differ in their micrometeorology and/or in the composition of ΣN_r, differences can be significant. For example, the daily cycle of March and April 2017 was clearly different to daily cycle of March and April 2018. During spring 2017, slight deposition fluxes were found whereas the ΣN_r exchange was close to neutral a year later. The median deposition was also slightly larger in March and April 2017 than in the year after (Fig. 5). In December 2017, the daily cycle was close to the zero line and positive fluxes were observed, although standard errors were relatively large ($\pm$ 11.5 ng N m^{-2} s^{-1} on average). In December 2016, slight deposition fluxes were observed for the entire daily cycle. The daily cycle of February 2018 showed high deposition values during the entire day, the highest values during the measurement campaign. Again, average standard error was relatively large ($\pm$ 19.9 ng N m^{-2} s^{-1}) for February 2018 compared to February 2017.

Figure S5 shows the median v_d to the corresponding fluxes. Values ranged between 0.2 and 0.5 cm s^{-1} for the entire campaign. In general, median v_d followed closely the seasonality of their corresponding fluxes (Fig. 5). During autumn and winter, v_d remained mostly stable. From May to September, the curve was approximately bell-shaped. Similar to the diurnal

fluxes, maximum v_d values were reached between 9:00 and 15:00 LT. During that time, values of v_d were close to 1 cm s^{-1} or even higher (Fig. S6).

3.2 Controlling factors of measured ΣN_r deposition velocities and resistances

The analysis of v_d and corresponding fluxes show that their diurnal pattern was characterized by lower deposition during the night and highest values around noon, in particular from May to September (Fig. 6 and Fig. S6). Micrometeorological parameters such as global radiation (Zöll et al., 2019), temperature (Wolff et al., 2010), humidity (Wyers and Erisman, 1998; Milford et al., 2001), and turbulence (Wolff et al., 2010), dry/wet leaf surfaces (Wyers and Erisman, 1998; Wentworth et al., 2016), and concentration of ΣN_r, especially changes in the concentration of the sub components, (Brümmer et al., 2013; Zöll et al., 2016) were reported to control the deposition of N_r compounds.

In order to investigate the effect of micrometeorology and vegetation on deposition, we further determined atmospheric and effective canopy resistances according to the equations given in Sec. 2.4. For visualizing the effect of turbulence on the fluxes, Fig. 7 shows the dependency of the measured fluxes on their concentrations for different u_* classes and global radiation (R_g) higher than 50 W m^{-2}.

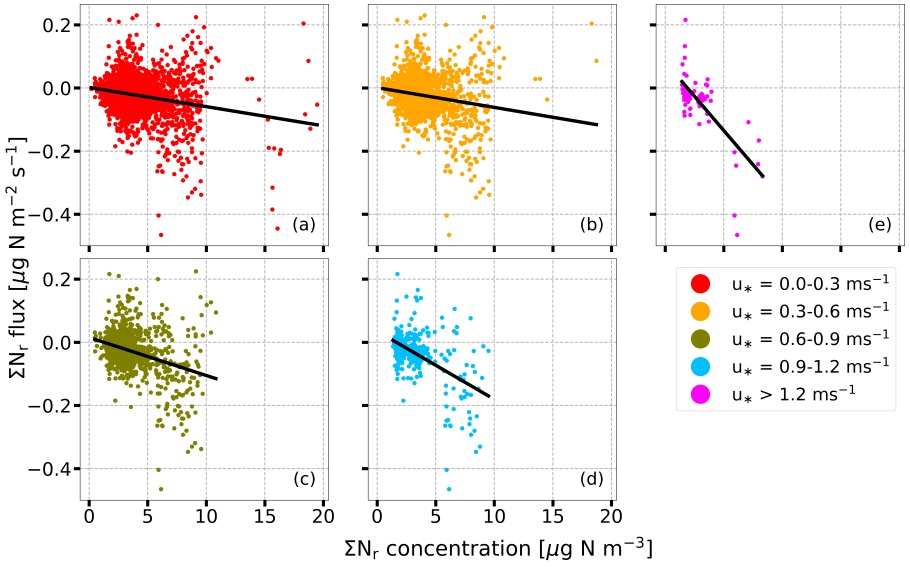

Figure 7. Dependency of measured concentrations on corresponding ΣN_r fluxes shown as scatter plots during daylight ($R_g > 50$ W m^{-2}). Colors indicate different u_* classes. Linear regressions between concentrations and fluxes are made for each u_* class indicated by black lines.

We found a decreasing slope with increasing u_*. The slope corresponds to v_d. Results of the linear regressions, v_d and squared correlations (R^2), are listed in Table 1. In addition, numbers of half-hours used for the regressions are given.

Table 1. Results of linear regressions from Fig. 7 for selected u_* ranges. The slope of the linear function corresponds to v_d, R^2 is the squared correlation of concentrations and fluxes, and n is the number of half-hours used for the regression.

u_* range [m s^{-1}]	v_d [cm s^{-1}]	R^2 [-]	n [-]
0.0–0.3	0.61	0.07	9085
0.3–0.6	0.63	0.05	6124
0.6–0.9	1.20	0.14	2296
0.9–1.2	2.16	0.28	485
> 1.2	4.34	0.51	79

For u_* values lower than 0.6 m s^{-1}, v_d was almost invariant. For u_* values higher than 0.6 m s^{-1} or even higher, an increase in v_d was found. Since R_a (Garland, 1977) and R_b (Jensen and Hummelshøj, 1995, 1997) decrease with increasing u_*, v_d increases. The highest R^2 was determined for u_* higher than 1.2 m s^{-1}. For other u_* ranges, correlations were negligible. However, only 79 half-hourly concentrations and fluxes were available for u_* values higher than 1.2 m s^{-1}. Considering the number of half-hours, atmospheric turbulence had an influence on the deposition of $\Sigma\mathrm{N_r}$ but u_* could not be solely responsible for the observed exchange of $\Sigma\mathrm{N_r}$.

Recently, Zöll et al. (2019) identified $\mathrm{R_g}$ as an important controlling factor for the $\Sigma\mathrm{N_r}$ fluxes at the measurement site from July to September. u_* did not emerge as controlling factor as reported by the authors. Figure S7 shows the daily cycle of concentration, $\mathrm{R_g}$, u_*, air temperature ($\mathrm{T_{air}}$), and v_d for the period from May to September. During that period, a clear diurnal pattern in v_d was observed with largest values around noon and lowest values during the night. Figure S8 is made for the same variables but for December, January, and February. During winter, v_d was almost equal and even lower during the day, which resulted in lower deposition of $\Sigma\mathrm{N_r}$ during winter. The different shapes of v_d were related to plant activity mainly controlled by $\mathrm{R_g}$.

Within the period of sufficient global radiation inducing $\Sigma\mathrm{N_r}$ exchange, we investigated the dependency of the $\Sigma\mathrm{N_r}$ deposition velocities and resistances on temperature, humidity, dry/wet leaf surface, and $\Sigma\mathrm{N_r}$ concentration. We separated half-hourly v_d and $R_\mathrm{c,eff}$ into groups of low and high temperature, humidity, and concentration according to their median. v_d and $R_\mathrm{c,eff}$ determined during rain were treated separately. In case of separating v_d and $R_\mathrm{c,eff}$ into groups of dry and wet leaf surfaces, we used the proposed calculation scheme of a leaf wetness boolean (see Sec. 2.2). No significant influence of the different installation heights on leaf surface wetness was found (see Fig. S9 and corresponding description in the supplement). Figures 8 and 9 show the results for v_d and $R_\mathrm{c,eff}$, respectively.

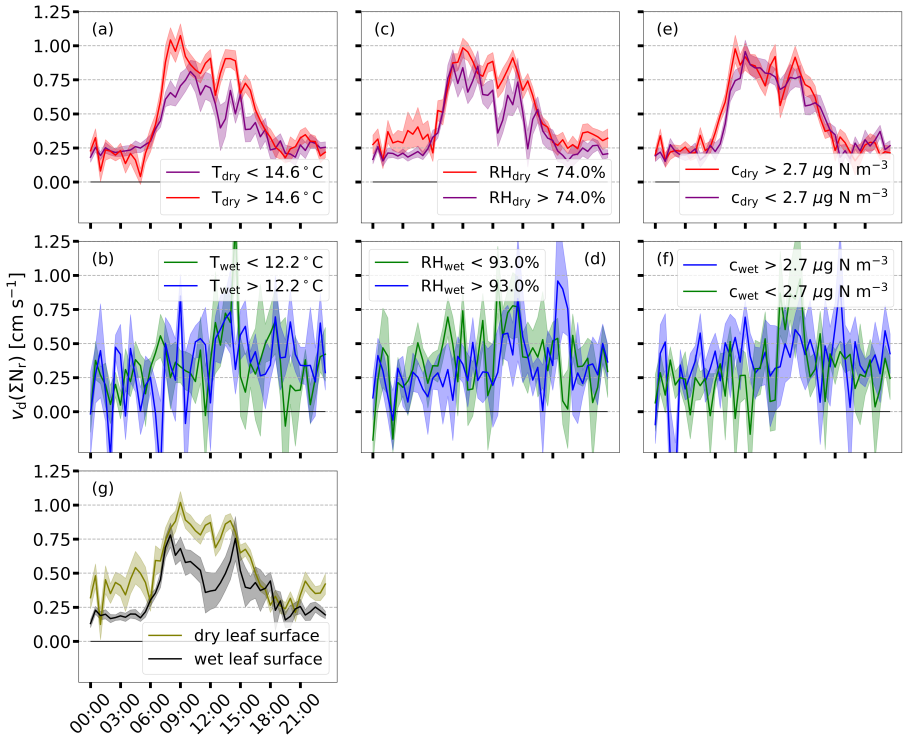

Figure 8. Mean daily cycle from May to September of v_d for low and high temperature, relative humidity, and concentration separated by precipitation in the conditions "dry" and "wet". Panel (a), (c), and (e) represent the case dry (no precipitation), (b), (d), and (f) the case wet. Median values of temperature, humidity, and concentration, which are derived for the same time period, are used as threshold values for separating v_d. In panel (g), the mean daily cycle of v_d for dry and wet leaf surfaces is shown. For classifying leaf surfaces as dry or wet, the scheme proposed in Sec. 2.2 is applied. The shaded areas represent the standard error of the mean.

In general, higher temperatures, less humidity, dry leaf surfaces, and dry conditions (no precipitation) enhanced deposition of $\Sigma\mathrm{N_r}$, and a clear diurnal pattern was observed for v_d with high values around noon and low, non-zero values in the night during dry conditions. During dawn/nighttime, deposition velocities exhibited no significant difference between the applied thresholds. Overall, no difference was found for low and high concentration regimes. In case of precipitation, v_d was reduced during daytime and exhibited a high variability for the entire day. No difference and distinct pattern could be found for low and high temperature, humidity, and concentration regimes during precipitation. During other times of the year, no diurnal pattern was observed during dry conditions. In those periods, v_d was almost constant and exhibited lower values during daylight compared to the May to September time frame. Occasionally, negative deposition velocities referring to emission of $\Sigma\mathrm{N_r}$ were recorded during times of lower radiation. Figure 9 is in accordance to Fig. 8 but for $R_{\mathrm{c,eff}}$.

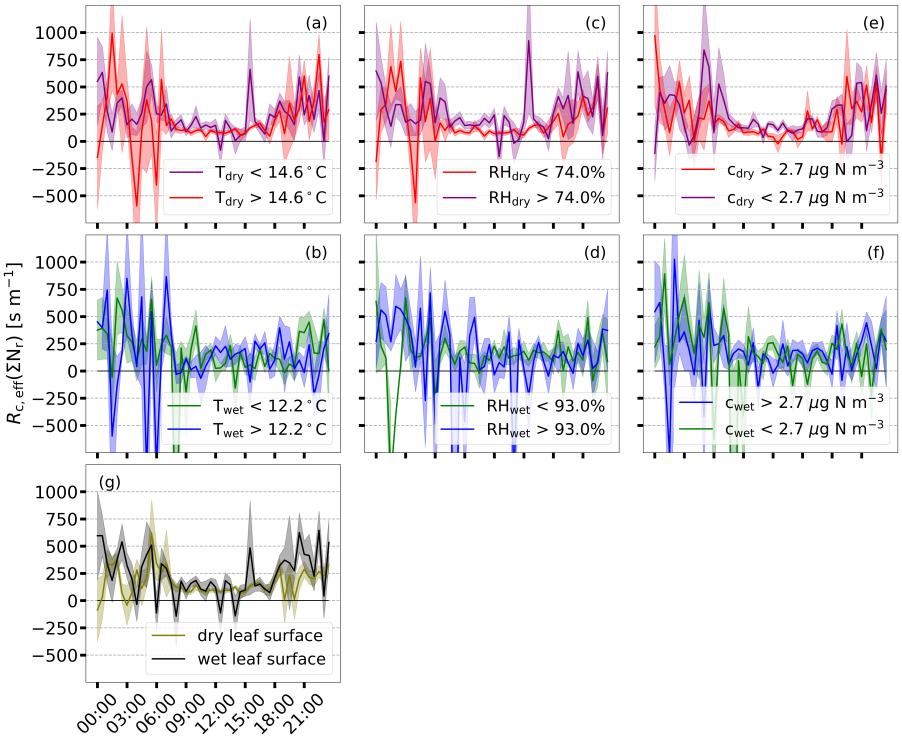

Figure 9. Mean daily cycle from May to September of $R_{c,eff}$ for low and high temperature, relative humidity, and concentration separated by precipitation in the conditions "dry" and "wet". Panel (a), (c), and (e) represent the case dry (no precipitation), (b), (d), and (f) the case wet. Median values of temperature, humidity, and concentration, which are derived for the same time period, are used as threshold values for separating $R_{c,eff}$. In panel (g), the mean daily cycle of $R_{c,eff}$ for dry and wet leaf surfaces is shown. For classifying leaf surfaces as dry or wet, the scheme proposed in Sec. 2.2 is applied. The shaded area represents the standard error of the mean.

$R_{c,eff}$ exhibited lowest values during the day and highest values at night. During nighttime, the variability in $R_{c,eff}$ was enhanced whereas $R_{c,eff}$ was almost stable during daylight. Only slight differences between the applied threshold were found. $R_{c,eff}$ was slightly lower at higher concentrations only for short periods during daylight, for example around noon. In case of relative humidity, $R_{c,eff}$ exhibited slightly lower values for less humid air. Temperature had nearly no effect on $R_{c,eff}$. During precipitation, no difference between the applied thresholds was found. Similar to v_d, $R_{c,eff}$ had a higher variability compared to dry conditions during the day resulting in higher uncertainties. Also phases with negative $R_{c,eff}$ values were observed during rain indicating emission of nitrogen from the canopy.

A similar analysis was made for R_a and R_b. During daylight, values of R_a and R_b were close to zero showing that v_d was mostly driven by the pattern of $R_{c,eff}$. Lower values of R_a and R_b were found for lower air humidity and higher temperature. In case of wet leaf surfaces, R_a and R_b were higher in the morning and evening. If wet leaf surfaces were excluded from the analysis, the differences for v_d and resistances to micrometeorological parameters diminished. Wet leaf surfaces reduced the uptake of ΣN_r at the measurement site. During the night or at lower radiation, R_a and R_b were comparable in magnitude to

$R_{c,eff}$. In autumn and winter, $R_{c,eff}$ showed partly negative values and no diurnal pattern. It should be noted that the shapes of the daily cycles of each parameter shown in Fig. 8 and 9 are almost similar for the chosen threshold values and differ only in amplitude.

3.3 Sensitivity of ΣN_r dry deposition sums to micrometeorological parameters

We found that higher temperatures, lower relative humidity, and no precipitation enhance deposition velocities and fluxes. The application of data-driven gap-filling methods like MDV (Falge et al., 2001) for estimating dry deposition could lead to biased results if micrometeorological conditions of the certain gap are different to fluxes used for filling the gap. We further applied a u_*-filter, which had removed preferentially smaller fluxes occurring at low turbulent conditions. Therefore, we determined dry deposition budgets with and without u_*-filter and conducted gap-filling with additional restrictions for temperature, humidity, and precipitation. Figure 10 shows the non gap-filled ΣN_r fluxes depicted as box plots and their cumulative sums with and without a u_*-filter if MDV is used as gap-filling approach. The threshold was set to 0.1 m s^{-1}, and the window for filling each gap was set to $\pm$5 days. Uncertainties of the gap-filled fluxes were estimated by the standard error of the mean. The total uncertainties were calculated as the sum of the standard errors.

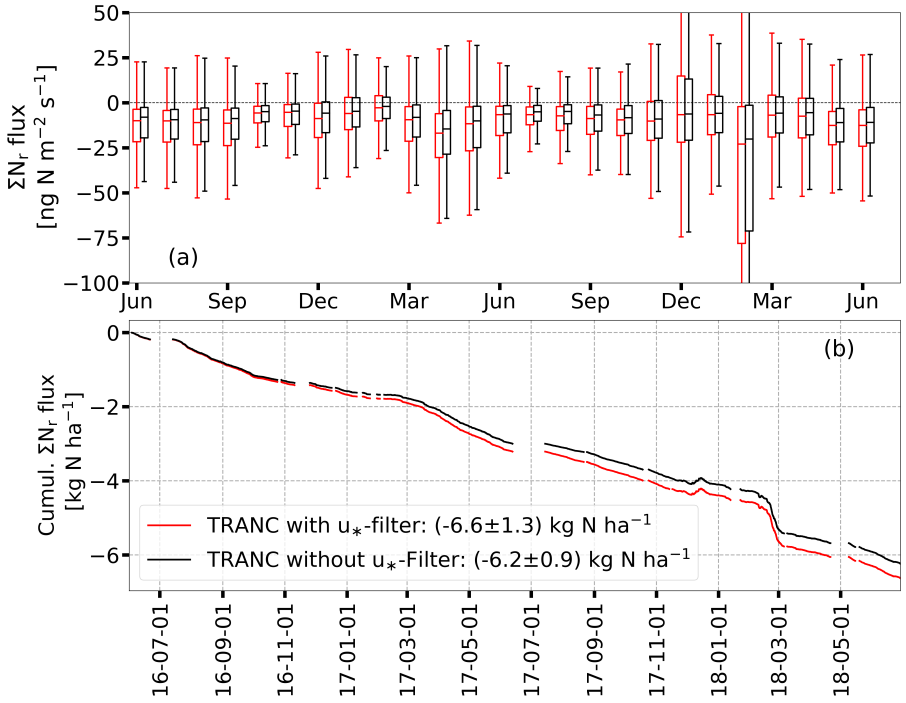

Figure 10. Panel (a) shows the non-gap filled ΣN_r fluxes depicted as box plots with (red) and without (black) u_*-filter in ng N m^{-2} s^{-1} (box frame = 25% to 75% interquartile ranges (IQR), bold line = median, whisker = 1.5· IQR). The threshold for u_* was set to 0.1 m s^{-1}. In panel (b), the cumulative dry deposition of ΣN_r is plotted for both cases in kg N ha^{-1}. For determining the cumulative curves, MDV was used as gap-filling method, and gaps were filled with fluxes being in a range of $\pm$5 days. Remaining gaps were not filled.

The difference in dry deposition was approximately 400 g N ha^{-1} after 2 years and is within the uncertainty range of the estimated dry depositions. Panel (a) of Fig. 10 shows that median depositions of the ΣN_r fluxes with u_*-filter were almost equal to or larger than the median depositions without u_*-filter. Figure 7 indicates that we measured large and small fluxes below 0.1 m s^{-1}. Thus, the applied u_* threshold removed not only small fluxes resulting in a consistent bias between the median depositions. The contribution of the water vapor correction (Eq. 1) to the estimated dry deposition was very low. ΣN_r interference fluxes were between -3 and -0.3 ng N $m^{-2}s^{-1}$. The uncertainty ranged between 0.0 and 0.5 ng N $m^{-2}s^{-1}$. Considering two years of TRANC flux measurements with MDV as gap-filling approach, the correction contributed with 132 g ha^{-1} to the estimated dry deposition of 6.6 kg ha^{-1}.

We further investigated the impact of temperature, humidity, and precipitation on the dry deposition sums of ΣN_r compared to the dry deposition without restrictions when using MDV as gap-filling approach since we found differences in the diurnal patterns of ΣN_r for micrometeorological parameters. Therefore, we considered only fluxes in the time frame of ± 5 days, at which temperature varied by $\pm 3°$C, humidity by $\pm 5\%$, or precipitation was recorded. Remaining, long-term gaps (see panel (b) of Fig. 10) were filled by a monthly average of the respective half-hourly value estimated from non-gap-filled fluxes (Fig. 6). Those averages were also calculated for low and high humidity and temperature regimes separated by their monthly median. The calculations were made with and without the application of a u_*-filter. Figure 11 shows the annual dry deposition of the measurement years from the beginning of June to end of May.

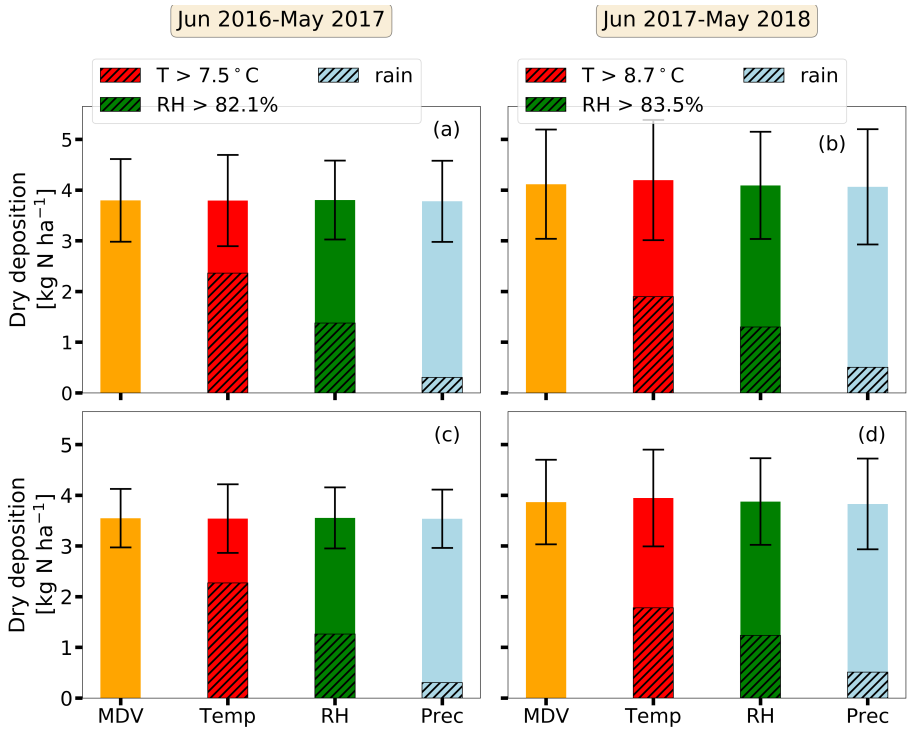

Figure 11. Annual ΣN_r dry deposition depicted as bar graphs from June to May in kg N ha^{-1}. For the orange bar, short-term gaps were filled with the MDV approach while using only fluxes in the time frame of ± 5 days. In case of the red, green, and blue bar, fluxes used for gap-filling have to additionally fulfilled criteria for temperature (± 3°C), humidity ($\pm 5\%$), or precipitation (wet or dry). Remaining gaps were replaced by monthly averages estimated for each half-hour calculated from the non-gap-filled fluxes. For the meteorological cases, monthly medians were used to determine those averages for low and high humidity and temperature regimes. (a) and (b) were made for fluxes with u_*-filter, (c) and (d) without it. The hatched area of the bars represent the dry deposition for temperatures and relative humidity values higher than the annual median shown in the legend and for wet conditions.

No significant difference could be found between the dry depositions sums for both measurement years. Consequently, the applied selection criteria did not lead to biased sums compared to the dry deposition determined without restrictions for meteorological parameters. Warm, drier conditions exhibited a higher contribution to the annual dry deposition, in particular for the first measurement year. During rain, dry deposition was less than 500 g N ha^{-1} per 12-month period. As shown before, a difference in the application of a u_*-filter exists but is within the uncertainty range. Dry deposition was higher in 2017/2018, which was related to the large deposition fluxes observed in February 2018. In total, we estimated 3.8 ± 0.8 kg N ha^{-1} and 4.1 ± 1.1 kg N ha^{-1} with the MDV approach (orange bar) and u_*-filter for 2016/2017 and 2017/2018, respectively.

Wet deposition was estimated from measurements of bulk and wet-only samplers. Table 2 shows the deposition estimates of NH_4^+-N, NO_3^--N, dissolved organic nitrogen (DON), and the resulting total nitrogen from wet deposition (TWD).

Table 2. Annual sums of NH_4^+-N, NO_3^--N, dissolved organic nitrogen (DON), and the resulting total wet depostion (TWD) from wet deposition samplers (bulk and wet-only). ∅ represents the average and s the standard deviation.

Sampler type	year	NH_4^+-N [kg ha^{-1}]	NO_3^- [kg ha^{-1}],	DON [kg ha^{-1}]	TWD [kg ha^{-1}]
Bulk	2016	3.8	3.4	1.5	8.7
	2017	3.4	3.4	0.7	7.5
	2018	2.8	2.7	0.7	6.2
	∅	3.3	3.2	1.0	7.5
	s	0.5	0.4	0.5	1.3
Wet-only	2016	4.0	3.6	0.9	8.5
	2017	3.4	3.6	0.5	7.5
	2018	2.9	2.6	0.6	6.1
	∅	3.4	3.3	0.7	7.4
	s	0.6	0.6	0.2	1.2

Differences between deposition estimates from bulk and wet-only samplers were not significant, and deposition estimates of NH_4^+-N and NO_3^--N were almost equal. Results from both sampling systems have in common that wet deposition of NH_4^+ and NO_3^- decreased from 2016 to 2018. In 2018, TWD was possibly lower due to the decreased amount of precipitation. Annual precipitation was approximately 200 mm lower in 2018 compared to 2017. In comparison to the results from dry deposition, wet deposition was about a factor two higher than dry deposition. Mean TWDs of wet-only samplers were 8.0 kg N ha^{-1} and 6.8 kg N ha^{-1} for the timeframe 2016/2017 and 2017/2018, respectively. In total, we got a total nitrogen deposition of 11.8 kg N ha^{-1} for 2016/2017 and 10.9 kg N ha^{-1} for 2017/2018.

4 Discussion

4.1 Interpretation of measured concentrations, deposition velocities, and fluxes

Measured half-hourly ΣN_r concentrations low relative to sites exposed to agricultural activities or urban environments. On average, we measured 5.5 ppb ΣN_r, 1.8 ppb NH_3, and 2.5 NO_x. Wintjen et al. (2020) determined an average ΣN_r concentration level of 21 ppb for a seminatural peatland, Brümmer et al. (2013) measured between 7 and 23 ppb as monthly averages above a cropland site, and Ammann et al. (2012) measured half-hourly ΣN_r concentrations ranging from less than 1 ppb to 350 ppb for a grassland site. Only for certain time periods, ΣN_r concentrations reached significantly higher values. During winter, NO_x increased due to emission from heating with fossil fuels and from combustion processes, for example through traffic and power plants. A generally lower mixing height, which is often observed during winter, also leads to higher ground-level concentrations of air pollutants. In spring and autumn, higher ΣN_r concentrations can be attributed to NH_3 emission from the

application of fertilizer and livestock farming in the surrounding environment (Beudert and Breit, 2010). NH_3 emissions from livestock farming in rural districts around the NPBW are approximately half of the emissions compared to rural districts located in the Donau-Inn valley (Beudert and Breit, 2010), who measured concentrations of NO_2 (2.1-4.8 ppb), NO (0.4-1.6 ppb) and NH_3 (1.4 ppb) at the same site. Those values for NO_2 and NO refer to 1992 until the end of 2008, NH_3 was measured from mid of 2003 to 2005. The low concentration level and seasonal variability of the ΣN_r compounds, in particular NH_3 and NO_2, are in agreement with Beudert and Breit (2010). Concentration values of NH_3 and NO_x are expectable for a site, which is some kilometers away from anthropogenic emission sources. Studies like Wyers and Erisman (1998); Horii et al. (2004); Wolff et al. (2010) conducted measurements of NH_3 and NO_2 above remote (mixed) forests and reported similar concentrations for those gases. In general, a comparison of ΣN_r concentrations and fluxes to other studies is difficult due to the measurement of the total nitrogen. Most studies, which have been published so far, focused only on a single or a few compounds of ΣN_r and are limited to selected sites and time periods of a few days or months. Only a few studies had been focusing on ΣN_r flux measurements using the EC method (see Ammann et al., 2012; Brümmer et al., 2013; Zöll et al., 2019; Wintjen et al., 2020).

Brümmer et al. (2013) measured ΣN_r exchange above an agricultural land. During unmanaged phases, fluxes were between -20 ng N m^{-2} s^{-1} and 20 ng N m^{-2} s^{-1}. Apart from management events, fluxes above the arable field site were closer to neutral conditions compared to our unmanaged forest site, which is mainly characterized by deposition fluxes and is therefore a larger sink for reactive nitrogen. Ammann et al. (2012) measured ΣN_r fluxes above a managed grassland. In the growing season, mostly deposition fluxes of -40 ng N m^{-2} s^{-1} were measured. The authors reported slightly increased deposition due to weak NO emission during that phase. Similar to Brümmer et al. (2013), the flux pattern observed by Ammann et al. (2012) is influenced by fertilizer application and thus, varying contributions of N_r compounds, for instance by bidirectionally exchanged NH_3 leading to both net emission and deposition phases of ΣN_r. Flux detection limit is almost equal to Zöll et al. (2019) but slightly higher than upper flux detection limits determined by Ammann et al. (2012) and Brümmer et al. (2013) for the same model. Despite the low signal-to-noise ratio at the measurement site, we were able to investigate the exchange pattern of ΣN_r and could estimate reliable dry deposition sums. To our knowledge, flux measurements of ΣN_r above mixed forests have not been carried out so far. We found that flux magnitude and diurnal flux pattern were similar to observations reported for individual N_r species above forests, e.g. NH_3 (Wyers and Erisman, 1998; Hansen et al., 2013, 2015), NO_2 (Horii et al., 2004; Geddes and Murphy, 2014), HNO_3 (Munger et al., 1996; Horii et al., 2006), and total ammonium (tot-NH_4^+) and total nitrate (tot-NO_3^-) (Wolff et al., 2010). As seen by the flux values and measurements of individual compounds, deposition prevails in the reported flux pattern, which corresponds to our measurements.

However, under certain circumstances regarding micrometeorology or the availability of ΣN_r compounds large deposition or emission fluxes can be observed. In February 2018, remarkably high ΣN_r concentrations and depositions were measured. Unfortunately, we had no DELTA measurements for February 2018, which could provide insights in the ambient concentrations of individual N_r species, but we found that SO_2 concentrations were unusually high (daily means up to 5.5 μg m^{-3}). During the entire campaign, we measured 1.0 μg m^{-3} SO_2 on average. SO_2 concentrations were slightly correlated with ΣN_r concentrations during the deposition period in February 2018. For the period of enhanced ΣN_r concentrations, a correlation of 0.29 was determined. Since reactions involving SO_2 and N_r species happen at different timescales, and ΣN_r consists of several,

chemically different compounds, low correlations are reasonable. SO_2 is rapidly converted to H_2SO_4. The latter is neutralized by NH_3 resulting in the formation of ammonium sulfate $(NH_4)_2SO_4$, a secondary inorganic aerosol. In the presence of HNO_3, NH_4NO_3 is formed by the reaction with NH_3. However, the formation of $(NH_4)_2SO_4$ is favored over the neutralization of HNO_3 at low NH_3 concentrations (Seinfeld and Pandis, 2006; Squizzato et al., 2013). Passive sampler measurements showed a low NH_3 concentration level in February 2018.

If the $[NH_4^+]/[SO_2^{-4}]$ molar ratio is lower than two (Squizzato et al., 2013), the aqueous or solid phase of $(NH_4)_2SO_4$ is prevailed aerosol form. At higher ratios, most of the sulfate is expended, and NH_3 is available for the neutralization of HNO_3. The existence of the solid phases depends highly on humidity, temperature, and the concentration of the constituents (Baek et al., 2004; Seinfeld and Pandis, 2006; Squizzato et al., 2013). The concentration of NH_3 needed for the formation of solid $(NH_4)_2SO_4$ is higher than values measured at our site, but the threshold depends on micrometeorology, for example, it reduces towards lower humidity levels (Seinfeld and Pandis, 2006). Presumably, not only $(NH_4)_2SO_4$ contributes to ΣN_r during February 2018 but compounds formed at lower ratios, e.g., ammonium bisulfate.

In December 2017, large emission fluxes were measured. Compared to 2016, significant difference in temperature and snowdepth were observed. Figure 12 shows recorded temperature, snow fall, concentrations, and estimated fluxes of ΣN_r from 6 December to 15 December for 2016 and 2017. Here, ± 3 days were chosen for filling the gaps in order to keep the short-term variability of the fluxes.

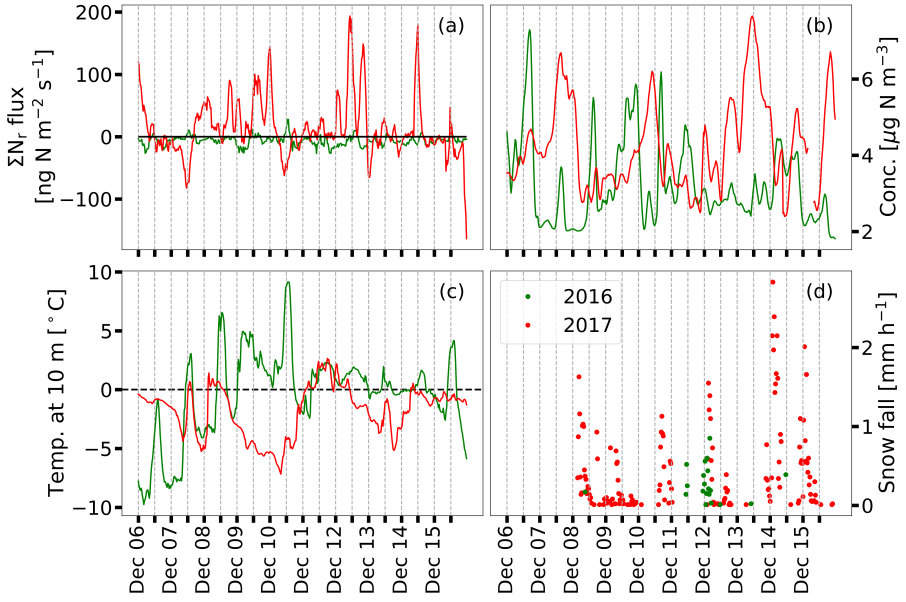

Figure 12. ΣN_r gap-filled fluxes (a), ΣN_r concentrations (b), air temperature at 10 m height above ground (c), and snow fall (d) from 6 December to 15 December for 2016 (green) and 2017 (red). Gaps are filled with the MDV approach with fluxes being in a range of ± 3 days. Fluxes and concentrations of ΣN_r were smoothed with a 3-h-running mean for better visualization.

In 2017, we observed substantial snow fall and a slower varying temperature compared to 2016 leading to significant snow depths compared to 2016. On the 1st of December, 1 cm and 20 cm snow depth were measured in the fetch of the tower for 2016 and 2017, respectively. Two weeks later, snow depth increased to 5 cm and 60 cm, respectively. In addition, temperatures were mostly higher than 0°C in December 2016. In 2017, temperatures were mostly below 0°C and only for one day above 0°C, and global radiation was mostly below 100 W m^{-2}.

Hansen et al. (2013) reported a change in the NH_3 flux pattern from deposition to emission due to the senescing of fallen leaves. The decomposition of litter leading to NH_3 emissions from the forest ground could be responsible for the observed emission fluxes of ΣN_r although the decomposition rate of litter is reduced at lower temperatures. However, the snow pack could act as an insulator and inhibited soil frost penetration. Therefore, decomposition of litter could have been happened under the snow pack. Kreyling et al. (2013) compared different snow treatments and their effect on decomposition. The authors observed nearly no soil frost penetration under snow insulation. The annual cellulose decomposition was greatly reduced for the snow removal treatment ($\sim 46\%$). An increasing mass loss rate was found under a deeper snow pack (Saccone et al., 2013) depending on the type and age of litter (Bokhorst et al., 2013). Due to a small snow depth in 2016, soil frost penetration had a higher potential to reduce the decomposition rate. In addition, temperatures were mostly above the freezing point leading to partial melting of the snow layer, which probably inhibited the release of hygroscopic N_r species such as NH_3. Thus, emission of nitrogen from the soil or the decomposition of leaves was probably reduced compared to 2017. The deeper snow layer promoted microbial activity, and the generally lower temperatures and radiation inhibited a melting of the upper snow layers. Thus, leakage of N_r species like NH_3 could have happened in December 2017. NO seems to be less responsible for the observed emission pattern following the findings of Medinets et al. (2016). They measured soil NO, N_2O, and CO_2 fluxes at a spruce forest during the 'cold' season (daily average temperature < 3°C). They found that NO fluxes were positively correlated to air and soil temperature. Snow cover was not identified as a determining factor for the NO fluxes by the authors, since NO efflux during snow cover and snow free periods were similar. However, the reported snow depth was only 4.6 cm on average. Soil frost penetration could have happened in the topsoil and lowered the NO emissions leading to lower correlation between NO and snow cover. As stated by the authors, different results had been published about the origin of NO emissions from snow covered soils (see Medinets et al., 2016, and references therein). An influence of NO either emitted from the snow pack or the soil cannot be fully excluded. A correlation of the measured fluxes with temperature was not found. This could be related to a time-shift between emission and dropping temperature. It has also to be considered that we measure approximately 30 m above the forest soil, and not only NO contributes ΣN_r. In addition, NO emitted from the forest floor can be converted to NO_2. Thus, low correlations were expected.

Our measurements further indicated that NO_x had the highest contribution to the measured ΣN_r concentrations. At the measurement height, the contribution of NO to NO_x was probably negligible. Median contribution of NO to NO_x is approximately 10% at 50 m. NO exhibits higher concentrations and fluxes close to the forest floor as shown by Rummel et al. (2002). Even if soil NO was converted to NO_2 it could still contribute to the measured ΣN_r flux except for the fraction that is removed by the canopy. NH_3 had strong presence in the ΣN_r concentration within the growing period of the plants, in particular during spring and summer. DELTA results revealed that gaseous N_r species have a high potential to influence the exchange pattern of

ΣN_r. The slight increase in HNO_3 and decrease of NH_4^+ can be related to the evaporation of NH_4NO_3 (Wyers and Duyzer, 1997; Van Oss et al., 1998). However, the findings of Tang et al. (2020) revealed that HNO_3 concentrations measured by the DELTA system using carbonate coated denuders may be significantly overestimated (45% on average) since HONO sticks also at those prepared surfaces. Thus, the HNO_3 contributions should be seen as an upper estimate. The comparison of the total N concentrations shows that the TRANC can adequately measure ΣN_r concentration. Obviously, not all components of ΣN_r were included in this comparison, for example, higher oxidized components like N_2O_5 could not be considered. As mentioned in Sec. 2.2, NO_2 had been measured at 50 m. However, Seok et al. (2013) found only slight differences in NO_2 concentrations above the canopy at a remote site. Thus, height differences in NO_2 are likely insignificant. Issues in the temperature stability or CO supply resulting in instabilities in the conversion efficiency of the TRANC, or a reduced sensitivity of the CLD could lead to differences to DELTA+NO_x. DELTA measurements report concentrations integrated over long time periods. Concentration peaks could not be collected sufficiently by the coated surfaces. The latter are exposed to environmental influences like temperature and moisture, and their sensitivity may reduce over time.

As shown in Fig. S5, median v_d of ΣN_r were low compared to deposition velocities determined for NH_3 or HNO_3 above other forests. Values range between 1.1 and 2.2 cm s^{-1} for NH_3 (see Schrader and Brümmer, 2014, and references therein) and between 2 and 8 cm s^{-1} for HNO_3 (Pryor and Klemm, 2004; Horii et al., 2006; Farmer and Cohen, 2008). v_d values reported for NO_2 are closer to v_d of ΣN_r. In the literature, v_d is between 0.015 and 0.51 cm s^{-1} for NO_2 (e.g., Rondon et al., 1993; Horii et al., 2004; Breuninger et al., 2013; Delaria et al., 2018, 2020). For tot-NH_4^+ and tot-NO_3^-, mean v_d of 3.4 cm s^{-1} and 4.2 cm s^{-1} were determined by Wolff et al. (2010), respectively. Since the analysis of the different N_r species contributing to the ΣN_r concentrations states NO_2 as the dominant compound, a similarity of v_d for ΣN_r to deposition velocities of NO_2 can be excepted. It further implicates a lower contribution of NH_3 than NO_2 to the measured flux.

4.2 Influence of micrometeorology and nitrogen concentrations on deposition and emission

4.2.1 Influence of R_g on ΣN_r exchange

Figure S7 and S8 showed that the shape of v_d and other micrometeorological variables is strongly correlated to R_g. Global radiation had been identified as an important 'driver' for the ΣN_r exchange, recently verified by an artificial neural network approach conducted by Zöll et al. (2019). The word 'driver' is a paraphrase of the expression 'controlling input variable' (Moffat et al., 2010). Drivers are identified by their correlation with the flux. As a remark, correlations could also be influenced by other parameters, which have not or could not considered by Zöll et al. (2019), for example chemical interactions of components contributing to ΣN_r.

As shown by Zöll et al. (2019), ΣN_r and CO_2 fluxes exhibited a similar daily cycle and showed a strong dependence on R_g during summer. The latter controls the opening of the stomata (Jarvis, 1976), i.e. lowers the stomatal resistance. Thus, photosynthesis controlling the CO_2 exchange through stomatal pathway appears to be the mechanism for controlling the ΣN_r exchange as compounds like NO_2 (Thoene et al., 1996) or NH_3 (Wyers and Erisman, 1998) are taken up by the stomatal pathway, too. However, ΣN_r compounds are not willingly absorbed by the plants as seen by the light response curves of

Zöll et al. (2019, Fig. 5). The light response curve of ΣN_r has a reversal instead of a saturation point as observed for CO_2 (Zöll et al., 2019). Consequently, a second mechanism, the stomatal compensation point firstly proposed by Farquhar et al. (1980) likely controls the uptake of the ΣN_r compounds. Basically, if the stomatal concentration is lower than the ambient concentration, deposition is observed. Thus, both parameters, the stomatal resistance and the stomatal compensation point, which are regulated by R_g and concentration, respectively, affect the uptake of ΣN_r. As further shown by Zöll et al. (2019), other parameters like u_* were not identified as important drivers for ΣN_r. Photochemistry and stomatal control appear to be more important than turbulent mixing. Radiation changes the composition of ΣN_r due to the formation of O_3. In addition, R_g had an influence on u_* as seen by their similar shapes in daily cycle (Fig. S7 and S8). The low correlations of ΣN_r fluxes to concentration for most of the selected u_* ranges show that atmospheric turbulence had a generally low influence on nitrogen deposition at the measurement site. Thus, u_* adds almost no additional information to the ΣN_r exchange and was not identified as important controlling factor for the ΣN_r exchange from July to September by Zöll et al. (2019). Similar conclusions can be drawn for temperature and relative humidity. They are also affected by light/energy input into the ecosystem and follow a similar diurnal pattern. It shows that R_g contains most of the information for the explanation of the ΣN_r fluxes.

It has to be noted that the study was conducted for ΣN_r at the same natural, unmanaged site from July to September. Micrometeorological parameters were controlled by natural processes. The low response to micrometeorological parameters may also related to other processes influencing the composition of ΣN_r, to opposing effects on N_r species, or effects happened on a shorter time scale such as molecular interactions between the ΣN_r compounds. R_g was not identified as primary controlling factor for NH_3 by Milford et al. (2001). Milford et al. (2001) measured NH_3 fluxes above moorland, which has a generally higher humidity level than our measurement site. They concluded that NH_3 exchange is mostly driven by canopy temperature, wetness, and ambient concentrations. Radiation was not identified as primary controlling factor by the authors. They found higher deposition of NH_3 through the cuticular than through the stomatal pathway. However, Zöll et al. (2019) found only minor improvements in their driver analysis if water vapor pressure deficit was considered as secondary driver. Additionally, we found that v_d was reduced for high ambient humidity and wet leaf surfaces. Since we measured NH_3 indirectly by the TRANC and above an ecosystem characterized by lower humidity than a peatland, R_g favoring the exchange through the stomatal pathway appears to be more important for ΣN_r at the measurement site.

4.2.2 Influence of N_r species on measured v_d

Zöll et al. (2019) further identified ΣN_r concentration as secondary driver for the ΣN_r deposition. The impact of increasing concentration on nitrogen (deposition) fluxes is well documented, for example, by Ammann et al. (2012) and Brümmer et al. (2013) for ΣN_r, by Horii et al. (2006) for NO_y, Horii et al. (2004) for NO_x, and by Zöll et al. (2016) for NH_3. We measured almost the same ΣN_r concentration for each season. Consequently, it was not only the change in the overall ΣN_r concentration that influences v_d. The changes in the contribution of the components of ΣN_r had a higher influence on v_d of ΣN_r than the overall concentration.

The higher nitrogen deposition in April 2017 (Fig. 5) compared to April 2018 was mainly related to gaps in flux time series. In 2018, we had no flux measurements from mid of April to the beginning of May. During that time, foliage began in 2018

providing uptake of ΣN_r compounds. Increased plant activity was caused by continously, high radiation values during daylight ($> 400\,W\,m^{-2}$) leading to higher temperatures in April 2018 ($\sim 11.0°C$) than in April 2017 ($\sim 6.0°C$). We further observed high NH_3 concentrations measured by passive samplers and the DELTA system for the same time. Elevated NH_3 concentrations were likely caused by emissions from agricultural management in the surrounding region. In 2017, leaf emergence began in early May. Thus, measured N deposition would have been higher in April 2018 than a year before presumably related to a lower stomatal resistance in 2018. Almost equal patterns of v_d and $R_{c,eff}$ were determined for May 2017 and 2018. The conditions for uptake of ΣN_r by the canopy were comparable. Consequently, the different contributions in NH_3 and conditions in radiation and temperature strongly affected v_d and $R_{c,eff}$ and therewith the deposition of ΣN_r.

In the summer of 2016 and 2017, differences in the ΣN_r median concentration were lower than 1 ppb. No remarkable differences in micrometeorology were found between summer 2016 and 2017. Figure 3 revealed that the contribution of components to ΣN_r differed between the investigated time periods. From July to September 2017, the mean NH_3 concentration was about $0.3\,\mu g\ N\ m^{-3}$ lower than a year before. HNO_3, NH_4^+, and NO_3^- were remarkably low in July 2017 compared to July 2016. In conclusion, the deviations in the median deposition were not related to differences in the ΣN_r concentration. The differences in the composition of ΣN_r affected v_d, in particular the canopy compensation point, more and therewith the uptake of ΣN_r.

However, we found that higher ΣN_r concentrations led to lower $R_{c,eff}$ during no precipitation around noon, which could be related to an increased energy input or/and to an increased contribution of nitrogen compounds like NH_3 to ΣN_r. Since the impact of concentration on $R_{c,eff}$ was comparatively low, it was superimposed by slight differences induced by R_a and R_b. Thus, ΣN_r concentration had almost no measurable net effect on v_d. Since we had measured the ΣN_r exchange in a low nitrogen environment, the influence of the stomatal compensation point on the uptake of N_r species may be reduced. Zöll et al. (2019) calculated a light response curve of ΣN_r for the same site. The increase in deposition got lower for R_g between 300 and $500\,W\,m^{-2}$ and reached a reversal point around $600\,W\,m^{-2}$. We found slight differences in $R_{c,eff}$ for the concentration threshold around noon, at times with the highest radiation. It shows that a stomatal compensation point exists but its influence is limited by the low, ambient nitrogen concentrations and radiation.

4.2.3 Seasonal changes in ΣN_r uptake capacity

Within the period of high incident radiation, in particular from May to September, a distinct diurnal pattern for v_d was observed, and no precipitation, high temperatures ($> 14.6°C$), low relative humidity ($< 74.0\%$), and dry leaf surfaces, were found to enhance the surface uptake, presumably through the stomatal pathway, of nitrogen during daylight. The observed differences in v_d for relative humidity and temperature were mostly related to R_a and R_b. $R_{c,eff}$ showed only a slight response to lower air humidity. Responses to the chosen temperature threshold and to dry leaf surfaces were not found.

During the rest of the year, no diurnal pattern was found under dry conditions (no precipitation) since stomata were likely closed, or requirements for stomatal deposition were not fulfilled (stomatal compensation point). Since we still observed a low, non-zero v_d but also short phases of ΣN_r emission during seasons with lower radiation, cuticular, soil, and turbulent driven processes were likely to be responsible for the ΣN_r exchange. In periods of reduced plant activity, for instance in winter and

autumn, the uptake through the stomatal pathway was greatly reduced or even inhibited due to reduced radiation or leaf area surfaces. Besides stomatal deposition, cuticular deposition is also an important pathway for ΣN_r compounds, which likely deposit on wet surfaces such as NH_3, HNO_3 or NH_4^+.

However, v_d was lower under wet conditions. Presumably, requirements for cuticular deposition were not fully met. Measurements of ΣN_r were conducted several kilometers away from nearby sources, and thus hydrophilic ΣN_r components could be washed out before air masses reached the site. We showed that the contribution and concentrations of N_r species, which can deposit on wet leaf surfaces, was comparatively low at the measurement site. Furthermore, those species were only indirectly measured, and wet leaf surfaces could be already saturated with water soluble N_r species leading to a high cuticular compensation point. These issues may reduce the cuticular contribution to exchange processes with the canopy. Presumably, cuticular deposition was probably not as important as stomatal deposition during the timeframe of high incident radiation, in particular from May to September. Stomatal deposition seems to be more important than other in-canopy uptake processes for the ecosystem in close proximity to the measurement site for those month.

The statement holds for the estimated fractions of N_r species found for this ecosystem. Ecosystems which are exposed to enhanced concentrations of NH_3 or nitrogen aerosols may differ in their uptake capacities. Wyers and Erisman (1998) measured highest NH_3 deposition if the canopy has a high water storage level (CWS) (> 2 mm). The deposition efficiency was reduced if CWS was higher than 0.25 mm but lower than 2 mm. By comparing different measurement years, they found differences in the deposition efficiency even if the canopy was saturated with water. They attributed the effect to the solubility of NH_3 in the water film. If canopy gets drier, evaporation of water occurs and the concentration of NH_3 increases in the water film. The cuticular resistance increases and deposition of NH_3 is reduced. Even emission of NH_3 was observed by Wyers and Erisman (1998), especially during the day when the canopy was dry, and NH_3 exchange was bidirectional. They showed that stomatal resistance was higher than canopy resistance. The authors identified cuticular deposition as more important for NH_3 as stomatal deposition. They measured an average NH_3 concentration of 5.2 μg m^{-3}. We measured 0.65 μg m^{-3} on average and found that the contribution of NH_3 to ΣN_r was comparatively low at the measurement site. If contribution of NH_3 or other soluble N_r species to ΣN_r is comparatively low, cuticular deposition is most likely reduced under wet conditions. The authors proposed that even under low ambient humidity leaf surfaces can exhibit high humidity due to the accumulation of particles. In case of conifer needles, Burkhardt et al. (1995) showed that particles deposit close to their stomata. Most of them are hygroscopic. Therewith, cuticular deposition seems to be possible even under low ambient humidity. However, our measurement site was several kilometers away from potential (anthropogenic) emission sources. Concentrations of NO_3^-, NH_4^+, sulphur dioxide (SO_2), and NO_x were comparatively low at the site, in particular during summer. Thus, stomatal deposition appears to be more important for ΣN_r under high temperatures, low relative humidity, and no precipitation. This conclusion is valid for months with sufficient light/energy input leading to an increased plant activity, i.e. from May to September. Within the other seasons, aerosol concentrations originating from natural or anthropogenic emission sources are probably higher resulting in a higher particle density on leaf surfaces promoting cuticular deposition.

Wolff et al. (2010) observed high deposition of tot-NH_4^+ and tot-NO_3^- during sunny days. During rain or fog, tot-NO_3^- exchange was almost neutral and emission was observed for tot-NH_4^+. They measured median concentration of 0.57, 0.12, 0.76,

and 0.45 μg m^{-3} for NH_3, HNO_3, NH_4^+, and NO_3^-, respectively. For the September months, we measured average concentrations of 0.76, 0.46, 0.50, and 0.78 μg m^{-3} for NH_3, HNO_3, NH_4^+, and NO_3^-, respectively. Measured tot-NO_3^- and tot-NH_4^+ of Wolff et al. (2010) exhibited a higher particle than gaseous contribution. At our measurement site, the gaseous contribution was higher than the values reported by Wolff et al. (2010). Median deposition velocities of tot-NO_3^- and tot-NH_4^+ were higher than values measured for ΣN_r at our site, and they found that deposition was mainly driven by aerodynamic resistance rather than by surface resistance, in particular during periods of high radiation. It shows that changes in the contribution of N_r species to ΣN_r lead to different deposition pathways.

4.3 Uncertainties in dry deposition estimates

Fluxes determined with the eddy-covariance method are exposed to systematic and random errors. Systematic errors are related to the design of the measurement setup and the instruments, data processing steps including calibration, tilt correction, detrending, and corrections due to low and high-frequency attenuation (Wintjen et al., 2020), and advection fluxes originating preferentially from non-homogeneous surfaces. Uncertainties from the measurement setup were likely caused by an insufficient pump performance, issues in temperature stability of the TRANC and CLD, sensitivity loss of the CLD, and problems in the O_2 and CO supply. Therefore, regular maintenance and continuous observation of instrument performance parameters such as TRANC temperature and flow rate were made. With manual screening of measured half-hours and the recording of these parameters, low-quality half-hours could be effectively excluded from analysis. A basic assumption for the EC method is that the terrain needs to be flat, and the canopy height and density should be uniform (Burba, 2013). These site criteria are not perfectly fulfilled at our measurement site. The site is located in a low mountain range and tree density is rather sparse south of the flux tower. Such diverse terrain characteristics could lead to unwanted turbulent fluctuations (non-stationarity of time series), which introduce noise in the cross-covariance function.

Random errors are mostly related to turbulence sampling errors (Finkelstein and Sims, 2001; Hollinger and Richardson, 2005; Loescher et al., 2006). An inadequate sample size results in an incomplete sampling of large-scale eddies, which compromises the cross-covariance of the vertical wind and the scalar of interest. The method of Finkelstein and Sims (2001) allows to quantify the random error of the measured fluxes ($F_{\mathrm{unc,meas}}$). In order to determine the effect of the random flux error on the estimated dry deposition sums, we used the method proposed by Pastorello et al. (2020):

$$F_{\mathrm{unc,cum_i}} = \sqrt{\Sigma_i^n (F_{\mathrm{unc,meas_i}})^2} \tag{7}$$

Using Eq. (7), we determined an uncertainty of 11 g N ha^{-1} for 2016/2017 and 21 g N ha^{-1} for 2017/2018 due to insufficient sampling of turbulent motion. The uncertainty related to u_* filtering is difficult to quantify since common approaches for estimating u_* thresholds, i.e. Moving Point Threshold (Reichstein et al., 2005) or Change Point Dectection (Barr et al., 2013), are designed for CO_2. Applying these threshold detection algorithms to N_r species is not suggested since their exchange patterns are characterized by a higher variability for different time scales. The chosen u_* threshold of 0.1 cm s^{-1} should be interpreted as minimal filter to exclude periods of insufficient turbulence (for details see Zöll et al., 2019, Sec. 2.4). In combination with the MDV approach as gap-filling method, the applied threshold may lead to biased dry deposition sums. As

seen in Fig. 10, the difference between dry deposition sums was within the error range of the dry deposition sum. Presumably, not only small fluxes were removed from the analysis by the u_*-filter. Figure 7 shows that large fluxes were observed at low turbulent conditions. We further showed that the contribution of the water vapor correction was negligible. Brümmer et al. (2013) and Ammann et al. (2012) reported a low contribution of the correction to their observed TRANC fluxes.

We calculated the uncertainties for the annual sums as standard error of the averaged flux, which is appropriate in case of the MDV method. We showed that the results when applying the MDV method were independent of the applied temperature, humidity, and precipitation criteria. The differences in v_d to micrometeorology were observed for a limited time period of the year. During other months, we found no influence of temperature, humidity, and precipitation on diurnal pattern of the $\Sigma\mathrm{N_r}$ fluxes. Thus, the dry deposition sums were almost equal for the applied micrometeorological criteria. The difference between the estimated dry depositions for the measurements was likely related to the large deposition occurring in February 2018. Presumably, the difference would have been even higher if flux measurements during the foliage period were available. It highlights the important role of radiation and the contribution of nitrogen compounds to the $\Sigma\mathrm{N_r}$ exchange at measurement site.

Using the MDV approach is recommended for gaps spanning over not more than a few days. Using statistical gap-filling approaches such as LUT, NLR, or MDV (Falge et al., 2001) for longer gaps, is not suggested. Statistical methods like MDV assume a periodic variability with high auto-correlation of fluxes. This assumption is mostly valid for CO_2, which have a distinctive daily cycle. Reactive gases mostly do not exhibit a clearly predictable flux pattern. Their flux variability depends on micrometeorological conditions and their chemical and physical properties sometimes leading to instationarities in data time series. Gap-filling methods based on inferential modeling or artificial neural networks may be a further valuable option, especially for long-term gaps - if models would be available. Monthly averages estimated for each half-hour do not account for short-term deposition or emission events. Since we measured mostly $\Sigma\mathrm{N_r}$ deposition at the measurement site, the applied gap-filling method for long-term gaps is somewhat justified. Also, biases due to the usage of statistical methods can be eliminated, for example, the shown effect of the u_*-filter on MDV. However, exchange patterns of every $\mathrm{N_r}$ species, at least the most important ones such as NO, NO_2, HNO_3, NH_3, NH_4^+, and NO_3^- have to be accurately modeled. In case of NH_3, stomatal and cuticular exchange is well documented (see references in Sec. 2.4). Investigations on other nitrogen compounds are still needed. As mentioned in Sec. 2.4, there are significant uncertainties in compensation points of NO_2 and HNO_3.

The results of wet deposition have shown that dry deposition contributes approximately one third to the total deposition, which is comparable to results of canopy outflow measurements conducted at the same site. The comparison of TRANC measurements with canopy outflow measurements will be shown the second part of this study. Wet deposition results from both sampler types were almost similar. It shows that deposition of sedimenting organic and inorganic particles is not relevant at the site.

5 Conclusions

Our study is the first one presenting 2.5 years flux measurements of total reactive atmospheric nitrogen (ΣN_r) measured with a custom-built converter called Total Reative Atmospheric nitrogen converter (TRANC) coupled to fast-response chemiluminescence detector (CLD) above a protected mixed forest.

A comparison of monthly averaged ΣN_r concentrations from the TRANC and DELTA (DEnuder for Long-Term Atmospheric sampling) and chemiluminescence measurements of nitrogen monoxide (NO) and nitrogen dioxide (NO_2) measurements showed a reasonable agreement in their seasonal patterns. On average, concentrations by the TRANC-CLD system were slightly higher ($\sim 0.3\,\mu$g N m^{-3}) showing that the TRANC-CLD system can adequately measure ΣN_r concentrations. Differences could be related to higher oxidized nitrogen compounds, which are not detected by the DELTA system, to a degrading of the denuder surfaces due to enviromental influences, issues in the conversion efficiency of the TRANC, etc. . Only nitrogen oxides (NO_x) and ammonia (NH_3) showed distinct seasonal changes in their concentrations whereas ΣN_r concentration remained stable through the year. NO_x exhibited highest concentrations during winter, NH_3 during spring and summer. In total, both gases had a mean contribution of 72.0% to the ΣN_r concentrations highlighting their importance for the observed ΣN_r exchange pattern.

We observed mostly deposition during 2.5 years of flux measurements. Median deposition ranged from -15 to -5 ng N m^{-2} s^{-1}. Deposition velocities followed the diurnal pattern of the fluxes, and median values ranged between 0.2 and 0.5 cm s^{-1}. Highest deposition was observed during the timeframe of high incident radiation, in particular from May to September. Our findings suggest that seasonal changes in the concentrations of the ΣN_r compounds and radiation were most likely responsible for the observed pattern of v_d. Within periods of high incident radiation, e.g. from May to September, deposition velocity (v_d) was elevated in presence of dry leaf surfaces, at a low humidity level, at higher temperatures, and during no precipitation. Calculated effective canopy resistance ($R_{c,eff}$) was slightly lower at lower humidity and higher concentrations of ΣN_r. Aerodynamic and boundary-layer resistances showed no significant contribution to v_d implicating a low influence of turbulent processes on the ΣN_r exchange during those times. During rain, v_d was greatly reduced or even negative resulting in emission of ΣN_r. During the year, uptake pathways for ΣN_r changed depending on the presence of individual ΣN_r compounds and micrometeorological conditions. Stomatal deposition seemed to be prevailing mostly from May to September. During the rest of the year, cuticular, soil, or turbulent processes appeared to be most responsible for the ΣN_r exchange.

From June 2016 to May 2017 and June 2017 to May 2018, we estimated dry deposition sums of 3.8$\pm$0.8 kg N ha^{-1} and 4.1$\pm$1.1 kg N ha^{-1}, respectively. Influences of temperature, humidity, friction velocity, or precipitation were in the uncertainty ranges of the estimated dry depositions sums. Using other gap-filling approaches based on inferential modeling or artificial neural networks for long-term gaps, is a valuable option. Also, biases related to the usage friction velocity thresholds, which potentially removes lower fluxes from the analysis and therefore affects data-driven gap-filling methods, will be avoided. Mean total wet deposition were 8.0 kg N ha^{-1} and 6.8 kg N ha^{-1} for the timeframes 2016/2017 and 2017/2018, respectively. The reduction in wet deposition was most likely related to the reduced precipitation in 2018. In the first and second measurement year, we determined 11.8 kg N ha^{-1} and 10.9 kg N ha^{-1} as total nitrogen deposition, respectively.

The data set presented in this study provides an unique opportunity for a comparison to deposition models. In the second part of this paper, a comparison of the acquired dataset to the performance of deposition models will be made. Modeled exchange dynamics will be discussed in regard to their biophysical controlling factors. Annual N budgets from measurements, modeling approaches using in-situ and modeled input parameters, and canopy outflow measurements will be shown.

Code and data availability. All data are available upon request from the first author of this study (pascal.wintjen@thuenen.de). Also, Python 3.7 code for flux data analysis can be requested from the first author.

Author contributions. PW, FS, and CB conceived the study. PW wrote the manuscript, carried out the measurements at the forest site, and conducted flux data analysis and interpretation. FS evaluated meteorological measurements. FS and MS provided insights in interpreting deposition velocities and resistances. BB performed the wet deposition analysis. CB installed the flux tower equipment and gave scientific advise to the overall data analysis and interpretation. All authors discussed the results and FS, MS, BB, and CB contributed to the manuscript.

Competing interests. The authors declare that they have no conflict of interest.

Acknowledgements. Funding by the German Environment Agency (UBA) (project FORESTFLUX, support code FKZ 3715512110) and by the German Federal Ministry of Education and Research (BMBF) within the framework of the Junior Research Group NITROSPHERE (support code FKZ 01LN1308A) is greatly acknowledged. We thank Undine Zöll for scientific and logistical help, Jeremy Rüffer and Jean-Pierre Delorme for excellent technical support, Ute Tambor, Andrea Niemeyer, and Dr. Daniel Ziehe for conducting laboratory analyses of denuder and filter samples, and the Bavarian Forest Nationalpark (NPBW) Administration, namely Wilhelm Breit and Ludwig Höcker for technical and logistical support at the measurement site.

References

Ammann, C., Wolff, V., Marx, O., Brümmer, C., and Neftel, A.: Measuring the biosphere-atmosphere exchange of total reactive nitrogen by eddy covariance, Biogeosciences, 9, 4247–4261, https://doi.org/10.5194/bg-9-4247-2012, http://www.biogeosciences.net/9/4247/2012/, 2012.

Aubinet, M., Vesala, T., and Papale, D., eds.: Eddy Covariance: A Practical Guide to Measurement and Data Analysis, Springer Science+Business Media B.V. 2012, Dordrecht, The Netherlands, 2012.

Baek, B. H., Aneja, V. P., and Tong, Q.: Chemical coupling between ammonia, acid gases, and fine particles, Environmental Pollution, 129, 89–98, https://doi.org/https://doi.org/10.1016/j.envpol.2003.09.022, https://www.sciencedirect.com/science/article/pii/S0269749103003816, 2004.

Barr, A., Richardson, A., Hollinger, D., Papale, D., Arain, M., Black, T., Bohrer, G., Dragoni, D., Fischer, M., Gu, L., Law, B., Margolis, H., McCaughey, J., Munger, J., Oechel, W., and Schaeffer, K.: Use of change-point detection for friction–velocity threshold evaluation in eddy-covariance studies, Agricultural and Forest Meteorology, 171-172, 31–45, https://doi.org/https://doi.org/10.1016/j.agrformet.2012.11.023, https://www.sciencedirect.com/science/article/pii/S0168192312003607, 2013.

Behrendt, T., Veres, P. R., Ashuri, F., Song, G., Flanz, M., Mamtimin, B., Bruse, M., Williams, J., and Meixner, F. X.: Characterisation of NO production and consumption: new insights by an improved laboratory dynamic chamber technique, Biogeosciences, 11, 5463–5492, https://doi.org/10.5194/bg-11-5463-2014, https://bg.copernicus.org/articles/11/5463/2014/, 2014.

Beudert, B. and Breit, W.: Integrated Monitoring Programm an der Meßstelle Forellenbach im Nationalpark Bayerischer Wald, Untersuchungen zu Prozessen und Räumen der Hochwasserbildung im Forellenbachgebiets, Förderkennzeichen 351 01 012. Nationalparkverwaltung Bayerischer Wald, Sachgebiet IV, techreport, Umweltbundesamt, http://docplayer.org/80741933-Integrated-monitoring-programm-an-der-messstelle-forellenbach-im-nationalpark-bayerischer-wald.html, 2008.

Beudert, B. and Breit, W.: Integrated Monitoring Programm an der Meßstelle Forellenbach im Nationalpark Bayerischer Wald, Untersuchungen zum Stickstoffeintrag und zum wassergebundenen Stickstoffhaushalt des Forellenbachgebiets, Förderkennzeichen 351 01 012. Nationalparkverwaltung Bayerischer Wald, Sachgebiet IV, techinal report, Umweltbundesamt, Dessau-Roßlau, Germany, http://www.umweltbundesamt.de/sites/default/files/medien/370/dokumente/ece_im_forellenbach_berichtsjahr_2009.pdf, 2010.

Beudert, B. and Breit, W.: Kronenraumbilanzen zur Abschätzung der Stickstoffgesamtdeposition in Waldökosysteme des Nationalparks Bayerischer Wald, techninal report, Umweltbundesamt, Dessau-Roßlau, Germany, https://www.umweltbundesamt.de/sites/default/files/medien/370/dokumente/kronenraumbilanzen_stickstoffgesamtdeposition_nationalpark_bayerisches_wald_-_berichtsjahr_2013_im_forellenbach.pdf, 2014.

Beudert, B., Bernsteinová, J., Premier, J., and Bässler, C.: Natural disturbance by bark beetle offsets climate change effects on streamflow in headwater catchments of the Bohemian Forest, Silva Gabreta, 24, 21–45, https://www.npsumava.cz/wp-content/uploads/2019/06/2_sg_24_beudertetal.pdf, 2018.

Bokhorst, S., Metcalfe, D. B., and Wardle, D. A.: Reduction in snow depth negatively affects decomposers but impact on decomposition rates is substrate dependent, Soil Biology and Biochemistry, 62, 157–164, https://doi.org/j.soilbio.2013.03.016, https://www.sciencedirect.com/science/article/pii/S0038071713001041, 2013.

Breuninger, C., Meixner, F. X., and Kesselmeier, J.: Field investigations of nitrogen dioxide (NO_2) exchange between plants and the atmosphere, Atmospheric Chemistry and Physics, 13, 773–790, https://doi.org/10.5194/acp-13-773-2013, https://acp.copernicus.org/articles/13/773/2013/, 2013.

Brümmer, C., Marx, O., Kutsch, W., Ammann, C., Wolff, V., Flechard, C. R., and Freibauer, A.: Fluxes of total reactive atmospheric nitrogen (ΣN_r) using eddy covariance above arable land, Tellus B: Chemical and Physical Meteorology, 65, 19 770, https://doi.org/10.3402/tellusb.v65i0.19770, https://doi.org/10.3402/tellusb.v65i0.19770, 2013.

Burba, G.: Eddy Covariance Method for Scientific, Industrial, Agricultural and Regulatory Applications: A Field Book on Measuring Ecosystem Gas Exchange and Areal Emission Rates, LI-COR Biosciences, Lincoln, Nebraska, USA, 2013.

Burkhardt, J., Peters, K., and Crossley, A.: The presence of structural surface waxes on coniferous needles affects the pattern of dry deposition of fine particles, Journal of Experimental Botany, 46, 823–831, 1995.

Chaparro-Suarez, I., Meixner, F., and Kesselmeier, J.: Nitrogen dioxide (NO2) uptake by vegetation controlled by atmospheric concentrations and plant stomatal aperture, Atmospheric Environment, 45, 5742–5750, https://doi.org/https://doi.org/10.1016/j.atmosenv.2011.07.021, https://www.sciencedirect.com/science/article/pii/S1352231011007461, 2011.

Civerolo, K. L. and Dickerson, R. R.: Nitric oxide soil emissions from tilled and untilled cornfields, Agricultural and Forest Meteorology, 90, 307–311, https://doi.org/10.1016/S0168-1923(98)00056-2, http://www.sciencedirect.com/science/article/pii/S0168192398000562, 1998.

Dämmgen, U., Thöni, L., Lumpp, R., Gilke, K., Seitler, E., and Bullinger, M.: Feldexperiment zum Methodenvergleich von Ammoniak- und Ammonium-Konzentrationsmessungen in der Umgebungsluft, 2005 bis 2008 in Braunschweig, vol. 337 of *Landbauforschung : Sonderheft*, Johann Heinrich von Thünen-Institut, Braunschweig, https://www.openagrar.de/receive/timport_mods_00006160, jahresberichtskategorie: 10-M4;10-3, 2010.

Delany, A. C., Fitzjarrald, D. R., Lenschow, D. H., Pearson, R., Wendel, G. J., and Woodrufl, B.: Direct measurements of nitrogen oxides and ozone fluxes over grassland, Journal of Atmospheric Chemistry, 4, 429–444, https://doi.org/10.1007/BF00053844, https://doi.org/10.1007/BF00053844, 1986.

Delaria, E. R., Vieira, M., Cremieux, J., and Cohen, R. C.: Measurements of NO and NO_2 exchange between the atmosphere and *Quercus agrifolia*, Atmospheric Chemistry and Physics, 18, 14 161–14 173, https://doi.org/10.5194/acp-18-14161-2018, https://www.atmos-chem-phys.net/18/14161/2018/, 2018.

Delaria, E. R., Place, B. K., Liu, A. X., and Cohen, R. C.: Laboratory measurements of stomatal NO_2 deposition to native California trees and the role of forests in the NO_x cycle, Atmospheric Chemistry and Physics, 20, 14 023–14 041, https://doi.org/10.5194/acp-20-14023-2020, https://acp.copernicus.org/articles/20/14023/2020/, 2020.

Durham, J. and Stockburger, L.: Nitric acid-air diffusion coefficient: Experimental determination, Atmospheric Environment (1967), 20, 559–563, https://doi.org/0004-6981(86)90098-3, https://www.sciencedirect.com/science/article/pii/0004698186900983, 1986.

Erisman, J. W. and Wyers, G. P.: Continuous measurements of surface exchange of SO_2 and NH_3; Implications for their possible interaction in the deposition process, Atmospheric Environment. Part A. General Topics, 27, 1937–1949, https://doi.org/10.1016/0960-1686(93)90266-2, http://linkinghub.elsevier.com/retrieve/pii/0960168693902662, 1993.

Erisman, J. W., Van Pul, A., and Wyers, P.: Parametrization of surface resistance for the quantification of atmospheric deposition of acidifying pollutants and ozone, Atmospheric Environment, 28, 2595–2607, https://doi.org/10.1016/1352-2310(94)90433-2, http://www.sciencedirect.com/science/article/pii/1352231094904332, 1994.

Erisman, J. W., Galloway, J. N., Seitzinger, S., Bleeker, A., Dise, N. B., Petrescu, A. M., Leach, A. M., and de Vries, W.: Consequences of human modification of the global nitrogen cycle, Philosophical Transactions of the Royal Society London B: Biological Sciences, 368, 20130 116, https://doi.org/10.1098/rstb.2013.0116, https://royalsocietypublishing.org/doi/abs/10.1098/rstb.2013.0116, 2013.

Eugster, W. and Hesterberg, R.: Transfer resistances of NO_2 determined from eddy correlation flux measurements over a litter meadow at a rural site on the swiss plateau, Atmospheric Environment, 30, 307–311, https://doi.org/10.1016/1352-2310(95)00418-1, http://www.sciencedirect.com/science/article/pii/1352231095004181, 1996.

Falge, E., Baldocchi, D., Olson, R., Anthoni, P., Aubinet, M., Bernhofer, C., Burba, G., Ceulemans, R., Clement, R., Dolman, H., Granier, A., Gross, P., Grünwald, T., Hollinger, D., Jensen, N.-O., Katul, G., Keronen, P., Kowalski, A., Lai, C. T., Law, B. E., Meyers, T., Moncrieff, J., Moors, E., Munger, J., Pilegaard, K., Üllar Rannik, Rebmann, C., Suyker, A., Tenhunen, J., Tu, K., Verma, S., Vesala, T., Wilson, K., and Wofsy, S.: Gap filling strategies for defensible annual sums of net ecosystem exchange, Agricultural and Forest Meteorology, 107, 43–69, https://doi.org/10.1016/S0168-1923(00)00225-2, http://www.sciencedirect.com/science/article/pii/S0168192300002252, 2001.

Famulari, D., Fowler, D., Hargreaves, K., Milford, C., Nemitz, E., Sutton, M. A., and Weston, K.: Measuring Eddy Covariance Fluxes of Ammonia Using Tunable Diode Laser Absorption Spectroscopy, Water, Air, & Soil Pollution: Focus, 4, 151–158, https://doi.org/10.1007/s11267-004-3025-1, http://link.springer.com/10.1007/s11267-004-3025-1, 2004.

Farmer, D. K. and Cohen, R. C.: Observations of HNO_3, Σ AN, Σ PN and NO_2 fluxes: evidence for rapid HO_x chemistry within a pine forest canopy, Atmospheric Chemistry and Physics, 8, 3899–3917, https://doi.org/10.5194/acp-8-3899-2008, https://www.atmos-chem-phys.net/8/3899/2008/, 2008.

Farmer, D. K., Wooldridge, P. J., and Cohen, R. C.: Application of thermal-dissociation laser induced fluorescence (TD-LIF) to measurement of HNO_3, Σ alkyl nitrates, Σ peroxy nitrates, and NO_2 fluxes using eddy covariance, Atmospheric Chemistry and Physics, 6, 3471–3486, https://doi.org/10.5194/acp-6-3471-2006, https://www.atmos-chem-phys.net/6/3471/2006/, 2006.

Farmer, D. K., Kimmel, J. R., Phillips, G., Docherty, K. S., Worsnop, D. R., Sueper, D., Nemitz, E., and Jimenez, J. L.: Eddy covariance measurements with high-resolution time-of-flight aerosol mass spectrometry: a new approach to chemically resolved aerosol fluxes, Atmospheric Measurement Techniques, 4, 1275–1289, https://doi.org/10.5194/amt-4-1275-2011, https://www.atmos-meas-tech.net/4/1275/2011/, 2011.

Farquhar, G. D., Firth, P. M., Wetselaar, R., and Weir, B.: On the Gaseous Exchange of Ammonia between Leaves and the Environment: Determination of the Ammonia Compensation Point, Plant Physiology, 66, 710–714, https://doi.org/10.1104/pp.66.4.710, http://www.plantphysiol.org/content/66/4/710, 1980.

Ferm, M.: A Sensitive Diffusional Sampler, Report L91-172, Swedish Environmental Research Institute, Gothenburg, 1991.

Ferrara, R. M., Loubet, B., Di Tommasi, P., Bertolini, T., Magliulo, V., Cellier, P., Eugster, W., and Rana, G.: Eddy covariance measurement of ammonia fluxes: Comparison of high frequency correction methodologies, Agricultural and Forest Meteorology, 158-159, 30–42, https://doi.org/10.1016/j.agrformet.2012.02.001, https://doi.org/10.1016/j.agrformet.2012.02.001, 2012.

Ferrara, R. M., Di Tommasi, P., Famulari, D., and Rana, G.: Limitations of an Eddy-Covariance System in Measuring Low Ammonia Fluxes, Boundary-Layer Meteorology, https://doi.org/10.1007/s10546-021-00612-6, https://doi.org/10.1007/s10546-021-00612-6, 2021.

Finkelstein, P. L. and Sims, P. F.: Sampling error in eddy correlation flux measurements, Journal of Geophysical Research: Atmospheres, 106, 3503–3509, https://doi.org/10.1029/2000JD900731, https://agupubs.onlinelibrary.wiley.com/doi/abs/10.1029/2000JD900731, 2001.

Flechard, C. R., Fowler, D., Sutton, M. A., and Cape, J. N.: A dynamic chemical model of bi-directional ammonia exchange between semi-natural vegetation and the atmosphere, Quarterly Journal of the Royal Meteorological Society, 125, 2611–2641, https://doi.org/10.1002/qj.49712555914, https://rmets.onlinelibrary.wiley.com/doi/abs/10.1002/qj.49712555914, 1999.

Flechard, C. R., Nemitz, E., Smith, R. I., Fowler, D., Vermeulen, A. T., Bleeker, A., Erisman, J. W., Simpson, D., Zhang, L., Tang, Y. S., and Sutton, M. A.: Dry deposition of reactive nitrogen to European ecosystems: a comparison of inferential models across the NitroEurope network, Atmospheric Chemistry and Physics, 11, 2703–2728, https://doi.org/10.5194/acp-11-2703-2011, 2011.

Flechard, C. R., Massad, R. S., Loubet, B., Personne, E., Simpson, D., Bash, J. O., Cooter, E. J., Nemitz, E., and Sutton, M. A.: Advances in understanding, models and parameterizations of biosphere-atmosphere ammonia exchange, Biogeosciences, 10, 5183–5225, https://doi.org/10.5194/bg-10-5183-2013, https://www.biogeosciences.net/10/5183/2013/, 2013.

Flechard, C. R., Ibrom, A., Skiba, U. M., de Vries, W., van Oijen, M., Cameron, D. R., Dise, N. B., Korhonen, J. F. J., Buchmann, N., Legout, A., Simpson, D., Sanz, M. J., Aubinet, M., Loustau, D., Montagnani, L., Neirynck, J., Janssens, I. A., Pihlatie, M., Kiese, R., Siemens, J., Francez, A.-J., Augustin, J., Varlagin, A., Olejnik, J., Juszczak, R., Aurela, M., Berveiller, D., Chojnicki, B. H., Dämmgen, U., Delpierre, N., Djuricic, V., Drewer, J., Dufrêne, E., Eugster, W., Fauvel, Y., Fowler, D., Frumau, A., Granier, A., Gross, P., Hamon, Y., Helfter, C., Hensen, A., Horváth, L., Kitzler, B., Kruijt, B., Kutsch, W. L., Lobo-do Vale, R., Lohila, A., Longdoz, B., Marek, M. V., Matteucci, G., Mitosinkova, M., Moreaux, V., Neftel, A., Ourcival, J.-M., Pilegaard, K., Pita, G., Sanz, F., Schjoerring, J. K., Sebastià, M.-T., Tang, Y. S., Uggerud, H., Urbaniak, M., van Dijk, N., Vesala, T., Vidic, S., Vincke, C., Weidinger, T., Zechmeister-Boltenstern, S., Butterbach-Bahl, K., Nemitz, E., and Sutton, M. A.: Carbon–nitrogen interactions in European forests and semi-natural vegetation – Part 1: Fluxes and budgets of carbon, nitrogen and greenhouse gases from ecosystem monitoring and modelling, Biogeosciences, 17, 1583–1620, https://doi.org/10.5194/bg-17-1583-2020, https://www.biogeosciences.net/17/1583/2020/, 2020.

Fowler, D., Flechard, C., Skiba, U., Coyle, M., and Cape, J. N.: The Atmospheric Budget of Oxidized Nitrogen and Its Role in Ozone Formation and Deposition, The New Phytologist, 139, 11–23, http://www.jstor.org/stable/2588244, 1998.

Galloway, J. N., Aber, J. D., Erisman, J. W., Seitzinger, S. P., Howarth, R. W., Cowling, E. B., and Cosby, B. J.: The Nitrogen Cascade, BioScience, 53, 341–356, https://doi.org/10.1641/0006-3568(2003)053[0341:TNC]2.0.CO;2, https://doi.org/10.1641/0006-3568(2003)053[0341:TNC]2.0.CO;2, 2003.

Garland, J. A.: The Dry Deposition of Sulphur Dioxide to Land and Water Surfaces, Proceedings of the Royal Society A: Mathematical, Physical and Engineering Sciences, 354, 245–268, https://doi.org/10.1098/rspa.1977.0066, https://royalsocietypublishing.org/doi/abs/10.1098/rspa.1977.0066, 1977.

Geddes, J. A. and Murphy, J. G.: Observations of reactive nitrogen oxide fluxes by eddy covariance above two midlatitude North American mixed hardwood forests, Atmospheric Chemistry and Physics, 14, 2939–2957, https://doi.org/10.5194/acp-14-2939-2014, https://acp.copernicus.org/articles/14/2939/2014/, 2014.

Gessler, A., Rienks, M., and Rennenberg, H.: NH3 and NO2 fluxes between beech trees and the atmosphere - correlation with climatic and physiological parameters, New Phytologist, 147, 539–560, https://doi.org/10.1046/j.1469-8137.2000.00712.x, http://doi.wiley.com/10.1046/j.1469-8137.2000.00712.x, 2000.

Gessler, A., Rienks, M., and Rennenberg, H.: Stomatal uptake and cuticular adsorption contribute to dry deposition of NH_3 and NO_2 to needles of adult spruce (Picea abies) trees, New Phytologist, 156, 179–194, https://doi.org/https://doi.org/10.1046/j.1469-8137.2002.00509.x, https://nph.onlinelibrary.wiley.com/doi/abs/10.1046/j.1469-8137.2002.00509.x, 2002.

Hansen, K., Sorensen, L. L., Hertel, O., Geels, C., Skjoth, C. A., Jensen, B., and Boegh, E.: Ammonia emissions from deciduous forest after leaf fall, Biogeosciences, 10, 4577–4589, https://doi.org/10.5194/bg-10-4577-2013, https://bg.copernicus.org/articles/10/4577/2013/, 2013.

Hansen, K., Pryor, S. C., Boegh, E., Hornsby, K. E., Jensen, B., and Sorensen, L. L.: Background concentrations and fluxes of atmospheric ammonia over a deciduous forest, Agricultural and Forest Meteorology, 214-215, 380–392, https://doi.org/10.1016/j.agrformet.2015.09.004, http://www.sciencedirect.com/science/article/pii/S0168192315007091, 2015.

Högberg, P.: Nitrogen impacts on forest carbon, Nature, 447, 781–782, https://doi.org/10.1038/447781a, https://doi.org/10.1038/447781a, 2007.

Hollinger, D. Y. and Richardson, A. D.: Uncertainty in eddy covariance measurements and its application to physiological models, Tree Physiology, 25, 873–85, https://www.ncbi.nlm.nih.gov/pubmed/15870055, 2005.

Horii, C. V., Munger, J. W., Wofsy, S. C., Zahniser, M., Nelson, D., and McManus, J. B.: Fluxes of nitrogen oxides over a temperate deciduous forest, Journal of Geophysical Research: Atmospheres, 109, https://doi.org/10.1029/2003JD004326, https://agupubs.onlinelibrary.wiley.com/doi/abs/10.1029/2003JD004326, 2004.

Horii, C. V., Munger, J. W., Wofsy, S. C., Zahniser, M., Nelson, D., and McManus, J. B.: Atmospheric reactive nitrogen concentration and flux budgets at a Northeastern US forest site, Agricultural and Forest Meteorology, 136, 159–174, https://doi.org/10.1016/j.agrformet.2006.03.005, http://www.sciencedirect.com/science/article/pii/S0168192306000888, 2006.

Hurkuck, M., Brümmer, C., Mohr, K., Grünhage, L., Flessa, H., and Kutsch, W. L.: Determination of atmospheric nitrogen deposition to a semi-natural peat bog site in an intensively managed agricultural landscape, Atmospheric Environment, 97, 296–309, https://doi.org/10.1016/j.atmosenv.2014.08.034, http://www.sciencedirect.com/science/article/pii/S1352231014006281, 2014.

Jarraud, M.: Guide to meteorological instruments and methods of observation (WMO-No. 8), World Meteorological Organization, Geneva, Switzerland, 2008.

Jarvis, P. G.: The Interpretation of the Variations in Leaf Water Potential and Stomatal Conductance Found in Canopies in the Field, Philosophical Transactions of the Royal Society B: Biological Sciences, 273, 593–610, https://doi.org/10.1098/rstb.1976.0035, http://rstb.royalsocietypublishing.org/content/273/927/593http://rstb.royalsocietypublishing.org/cgi/doi/10.1098/rstb.1976.0035, 1976.

Jensen, N. and Hummelshøj, P.: Derivation of canopy resistance for water vapor fluxes over a spruce forest, using a new technique for the viscous sublayer resistance (correction to vol. 73, p. 339, 1995), Agricultural and Forest Meteorology, 85, 289, https://doi.org/10.1016/S0168-1923(97)00024-5, http://www.sciencedirect.com/science/article/pii/S0168192397000245, 1997.

Jensen, N. O. and Hummelshøj, P.: Derivation of canopy resistance for water-vapor fluxes over a spruce forest, using a new technique for the viscous sublayer resistance, Agricultural and Forest Meteorology, 73, 339–352, https://doi.org/10.1016/0168-1923(94)05083-I, http://www.sciencedirect.com/science/article/pii/016819239405083I, 1995.

Kolle, O. and Rebmann, C.: EddySoft Documentation of a Software Package to Acquire and Process Eddy Covariance Data, techreport, MPI-BGC, https://repository.publisso.de/resource/frl:4414276-1/data, 2007.

Kreyling, J., Haei, M., and Laudon, H.: Snow removal reduces annual cellulose decomposition in a riparian boreal forest, Canadian Journal of Soil Science, 93, 427 – 433, https://doi.org/10.1139/CJSS2012-025, https://doi.org/10.1139/CJSS2012-025, 2013.

Krupa, S. V.: Effects of atmospheric ammonia (NH_3) on terrestrial vegetation: a review, Environmental Pollution, 124, 179–221, https://doi.org/10.1016/S0269-7491(02)00434-7, http://www.sciencedirect.com/science/article/pii/S0269749102004347, 2003.

Langford, B., Acton, W., Ammann, C., Valach, A., and Nemitz, E.: Eddy-covariance data with low signal-to-noise ratio: time-lag determination, uncertainties and limit of detection, Atmospheric Measurement Techniques, 8, 4197–4213, https://doi.org/10.5194/amt-8-4197-2015, https://www.atmos-meas-tech.net/8/4197/2015/, 2015.

Li, Y., Aneja, V. P., Arya, S. P., Rickman, J., Brittig, J., Roelle, P., and Kim, D. S.: Nitric oxide emission from intensively managed agricultural soil in North Carolina, Journal of Geophysical Research: Atmospheres, 104, 26 115–26 123, https://doi.org/10.1029/1999JD900336, https://agupubs.onlinelibrary.wiley.com/doi/abs/10.1029/1999JD900336, 1997.

Loescher, H. W., Law, B. E., Mahrt, L., Hollinger, D. Y., Campbell, J., and Wofsy, S. C.: Uncertainties in, and interpretation of, carbon flux estimates using the eddy covariance technique, Journal of Geophysical Research: Atmospheres, 111, https://doi.org/https://doi.org/10.1029/2005JD006932, https://agupubs.onlinelibrary.wiley.com/doi/abs/10.1029/2005JD006932, 2006.

LTER: Long Term Ecological Research (LTER) network, https://deims.org/993ed2fc-1cb0-4810-a619-8bcf78b6ecee, last access: 17 June 2020, 2020.

Ludwig, J., Meixner, F., Vogel, B., and Förstner, J.: Soil-air exchange of nitric oxide: An overview of processes, environmental factors, and modeling studies, Biogeochemistry, 52, 225–257, https://doi.org/10.1023/A:1006424330555, 2001.

Magnani, F., Mencuccini, M., Borghetti, M., Berbigier, P., Berninger, F., Delzon, S., Grelle, A., Hari, P., Jarvis, P. G., Kolari, P., Kowalski, A. S., Lankreijer, H., Law, B. E., Lindroth, A., Loustau, D., Manca, G., Moncrieff, J. B., Rayment, M., Tedeschi, V., Valentini, R., and Grace, J.: The human footprint in the carbon cycle of temperate and boreal forests, Nature, 447, 848–50, https://doi.org/10.1038/nature05847, https://www.ncbi.nlm.nih.gov/pubmed/17568744, 2007.

Marx, O., Brümmer, C., Ammann, C., Wolff, V., and Freibauer, A.: TRANC – a novel fast-response converter to measure total reactive atmospheric nitrogen, Atmospheric Measurement Techniques, 5, 1045–1057, https://doi.org/10.5194/amt-5-1045-2012, http://www.atmos-meas-tech.net/5/1045/2012/, 2012.

Massad, R. S., Nemitz, E., and Sutton, M. A.: Review and parameterisation of bi-directional ammonia exchange between vegetation and the atmosphere, Atmospheric Chemistry and Physics, 10, 10 359–10 386, https://doi.org/10.5194/acp-10-10359-2010, https://www.atmos-chem-phys.net/10/10359/2010/, 2010.

Massman, W. J.: A review of the molecular diffusivities of H2O, CO2, CH4, CO, O3, SO2, NH3, N2O, NO, and NO2 in air, O2 and N2 near STP, Atmospheric Environment, 32, 1111–1127, https://doi.org/10.1016/s1352-2310(97)00391-9, 1998.

Mauder, M. and Foken, T.: Impact of post-field data processing on eddy covariance flux estimates and energy balance closure, Meteorologische Zeitschrift, 15, 597–609, https://doi.org/10.1127/0941-2948/2006/0167, 2006.

Medinets, S., Gasche, R., Skiba, U., Schindlbacher, A., Kiese, R., and Butterbach-Bahl, K.: Cold season soil NO fluxes from a temperate forest: drivers and contribution to annual budgets, Environmental Research Letters, 11, 114 012, https://doi.org/10.1088/1748-9326/11/11/114012, https://doi.org/10.1088/1748-9326/11/11/114012, 2016.

Milford, C., Hargreaves, K. J., Sutton, M. A., Loubet, B., and Cellier, P.: Fluxes of NH_3 and CO_2 over upland moorland in the vicinity of agricultural land, Journal of Geophysical Research: Atmospheres, 106, 24 169–24 181, https://doi.org/10.1029/2001jd900082, http://doi.wiley.com/10.1029/2001JD900082, 2001.

Min, K.-E., Pusede, S. E., Browne, E. C., LaFranchi, B. W., Wooldridge, P. J., and Cohen, R. C.: Eddy covariance fluxes and vertical concentration gradient measurements of NO and NO_2 over a ponderosa pine ecosystem: observational evidence for within-canopy chemical removal of NO_x, Atmospheric Chemistry and Physics, 14, 5495–5512, https://doi.org/10.5194/acp-14-5495-2014, http://www.atmos-chem-phys.net/14/5495/2014/, 2014.

Moffat, A. M., Papale, D., Reichstein, M., Hollinger, D. Y., Richardson, A. D., Barr, A. G., Beckstein, C., Braswell, B. H., Churkina, G., Desai, A. R., Falge, E., Gove, J. H., Heimann, M., Hui, D. F., Jarvis, A. J., Kattge, J., Noormets, A., and Stauch, V. J.: Comprehensive comparison of gap-filling techniques for eddy covariance net carbon fluxes, Agricultural and Forest Meteorology, 147, 209–232, https://doi.org/10.1016/j.agrformet.2007.08.011, https://doi.org/10.1016/j.agrformet.2007.08.011, 2007.

Moffat, A. M., Beckstein, C., Churkina, G., Mund, M., and Heimann, M.: Characterization of ecosystem responses to climatic controls using artificial neural networks, Global Change Biology, 16, 2737–2749, https://doi.org/j.1365-2486.2010.02171.x, https://onlinelibrary.wiley.com/doi/abs/10.1111/j.1365-2486.2010.02171.x, 2010.

Moncrieff, J., Clement, R., Finnigan, J., and Meyers, T.: Averaging, Detrending, and Filtering of Eddy Covariance Time Series, pp. 7–31, Kluwer Academic, Dordrecht, https://doi.org/10.1007/1-4020-2265-4_2, https://doi.org/10.1007/1-4020-2265-4_2, 2004.

Moravek, A., Singh, S., Pattey, E., Pelletier, L., and Murphy, J. G.: Measurements and quality control of ammonia eddy covariance fluxes: A new strategy for high frequency attenuation correction, Atmospheric Measurement Techniques, 12, 6059–6078, https://doi.org/10.5194/amt-12-6059-2019, https://www.atmos-meas-tech.net/12/6059/2019/, 2019.

Munger, J. W., Wofsy, S. C., Bakwin, P. S., Fan, S. M., Goulden, M. L., Daube, B. C., Goldstein, A. H., Moore, K. E., and Fitzjarrald, D. R.: Atmospheric deposition of reactive nitrogen oxides and ozone in a temperate deciduous forest and a subarctic woodland: 1. Measurements and mechanisms, Journal of Geophysical Research-Atmospheres, 101, 12 639–12 657, https://doi.org/10.1029/96JD00230, https://agupubs.onlinelibrary.wiley.com/doi/abs/10.1029/96JD00230, 1996.

Neirynck, J. and Ceulemans, R.: Bidirectional ammonia exchange above a mixed coniferous forest, Environmental Pollution, 154, 424–38, https://doi.org/10.1016/j.envpol.2007.11.030, https://www.ncbi.nlm.nih.gov/pubmed/18258346, 2008.

Nemitz, E., Sutton, M. A., Schjoerring, J. K., Husted, S., and Wyers, G. P.: Resistance modelling of ammonia exchange over oilseed rape, Agricultural and Forest Meteorology, 105, 405–425, https://doi.org/10.1016/S0168-1923(00)00206-9, http://www.sciencedirect.com/science/article/pii/S0168192300002069, 2000.

Nemitz, E., Milford, C., and Sutton, M. A.: A two-layer canopy compensation point model for describing bi-directional biosphere-atmosphere exchange of ammonia, Quarterly Journal of the Royal Meteorological Society, 127, 815–833, https://doi.org/10.1002/qj.49712757306, https://rmets.onlinelibrary.wiley.com/doi/abs/10.1002/qj.49712757306, 2001.

Nemitz, E., Sutton, M. A., Wyers, G. P., and Jongejan, P. A. C.: Gas-particle interactions above a Dutch heathland: I. Surface exchange fluxes of NH_3, SO_2, HNO_3 and HCl, Atmospheric Chemistry and Physics, 4, 989–1005, https://doi.org/10.5194/acp-4-989-2004, https://www.atmos-chem-phys.net/4/989/2004/, 2004.

Nemitz, E., Jimenez, J. L., Huffman, J. A., Ulbrich, I. M., Canagaratna, M. R., Worsnop, D. R., and Guenther, A. B.: An Eddy-Covariance System for the Measurement of Surface/Atmosphere Exchange Fluxes of Submicron Aerosol Chemical Species—First Application Above an Urban Areas, Aerosol Science and Technology, 42, 636–657, https://doi.org/10.1080/02786820802227352, https://doi.org/10.1080/02786820802227352, 2008.

Pastorello, G., Trotta, C., and Canfora, E. e. a.: The FLUXNET2015 dataset and the ONEFlux processing pipeline for eddy covariance data, Scientific Data, 7, 225, https://doi.org/10.1038/s41597-020-0534-3, https://doi.org/10.1038/s41597-020-0534-3, 2020.

Paulson, C. A.: The Mathematical Representation of Wind Speed and Temperature Profiles in the Unstable Atmospheric Surface Layer, Journal of Applied Meteorology, 9, 857–861, https://doi.org/10.1175/1520-0450(1970)009<0857:Tmrows>2.0.Co;2, 1970.

Peake, E. and Legge, A. H.: Evaluation of methods used to collect air quality data at remote and rural sites in Alberta, Canada, in: Proc. 1987 EPA/APCA Symposium on Measurements of Toxic and Related Air Pollutants, APCA, 1987.

Peake, M.: A Preliminary Report on the Design and Testing of the KAPS (Kananaskis Atmospheric Pollutant Sampler) for the Collection of Acidic and Basic Gases and Fine Particles, Document 0012e/July 8/85. Typskript University Calgary, 1985.

Pryor, S. and Klemm, O.: Experimentally derived estimates of nitric acid dry deposition velocity and viscous sub-layer resistance at a conifer forest, Atmospheric Environment, 38, 2769–2777, https://doi.org/https://doi.org/10.1016/j.atmosenv.2004.02.038, https://www.sciencedirect.com/science/article/pii/S1352231004002158, 2004.

Reichstein, M., Falge, E., Baldocchi, D., Papale, D., Aubinet, M., Berbigier, P., Bernhofer, C., Buchmann, N., Gilmanov, T., Granier, A., Grünwald, T., Havránková, K., Ilvesniemi, H., Janous, D., Knohl, A., Laurila, T., Lohila, A., Loustau, D., Matteucci, G., Meyers, T., Miglietta, F., Ourcival, J.-M., Pumpanen, J., Rambal, S., Rotenberg, E., Sanz, M., Tenhunen, J., Seufert, G., Vaccari, F., Vesala, T., Yakir, D., and Valentini, R.: On the separation of net ecosystem exchange into assimilation and ecosystem respiration: review and improved

algorithm, Global Change Biology, 11, 1424–1439, https://doi.org/10.1111/j.1365-2486.2005.001002.x, https://onlinelibrary.wiley.com/doi/abs/10.1111/j.1365-2486.2005.001002.x, 2005.

Remde, A. and Conrad, R.: Role of nitrification and denitrification for NO metabolism in soil, Biogeochemistry, 12, 189–205, https://doi.org/110.1007/BF00002607, https://doi.org/10.1007/BF00002607, 1993.

Remde, A., Slemr, F., and Conrad, R.: Microbial production and uptake of nitric oxide in soil, FEMS Microbiology Letters, 62, 221–230, https://doi.org/https://doi.org/10.1016/0378-1097(89)90246-2, https://www.sciencedirect.com/science/article/pii/0378109789902462, 1989.

Rondón, A. and Granat, L.: Studies on the dry deposition of NO2 to coniferous species at low NO2 concentrations, Tellus B: Chemical and Physical Meteorology, 46, 339–352, https://doi.org/10.3402/tellusb.v46i5.15809, https://doi.org/10.3402/tellusb.v46i5.15809, 1994.

Rondon, A., Johansson, C., and Granat, L.: Dry Deposition of Nitrogen-Dioxide and Ozone to Coniferous Forests, Journal of Geophysical Research-Atmospheres, 98, 5159–5172, https://doi.org/Doi 10.1029/92jd02335, <GotoISI>://WOS:A1993KU06900024, 1993.

Rummel, U., Ammann, C., Gut, A., Meixner, F. X., and Andreae, M. O.: Eddy covariance measurements of nitric oxide flux within an Amazonian rain forest, Journal of Geophysical Research-Atmospheres, 107, LBA 17–1–LBA 17–9, https://doi.org/10.1029/2001JD000520, https://doi.org/10.1029/2001JD000520, 2002.

Saccone, P., Morin, S., Baptist, F., Bonneville, J.-M., Colace, M.-P., Domine, F., Faure, M., Geremia, R., Lochet, J., Poly, F., Lavorel, S., and Clèment, J.-C.: The effects of snowpack properties and plant strategies on litter decomposition during winter in subalpine meadows, Plant and Soil, 363, 215–229, https://doi.org/10.1007/s11104-012-1307-3, https://doi.org/10.1007/s11104-012-1307-3, 2013.

Schindlbacher, A., Zechmeister-Boltenstern, S., and Butterbach-Bahl, K.: Effects of soil moisture and temperature on NO, NO2, and N2O emissions from European forest soils, Journal of Geophysical Research-Atmospheres, 109, 1–12, https://doi.org/10.1029/2004jd004590, https://agupubs.onlinelibrary.wiley.com/doi/abs/10.1029/2004JD004590, 2004.

Schrader, F. and Brümmer, C.: Land Use Specific Ammonia Deposition Velocities: a Review of Recent Studies (2004–2013), Water, Air, and Soil Pollution, 225, 2114, https://doi.org/10.1007/s11270-014-2114-7, https://doi.org/10.1007/s11270-014-2114-7, 2014.

Schrader, F., Brümmer, C., Flechard, C. R., Wichink Kruit, R. J., van Zanten, M. C., Zöll, U., Hensen, A., and Erisman, J. W.: Non-stomatal exchange in ammonia dry deposition models: comparison of two state-of-the-art approaches, Atmospheric Chemistry and Physics, 16, 13 417–13 430, https://doi.org/10.5194/acp-16-13417-2016, https://www.atmos-chem-phys.net/16/13417/2016/, 2016.

Seinfeld, J. H. and Pandis, S. N.: Atmospheric Chemistry and Physics – From Air Pollution to Climate Change, John Wiley & Sons, New York, USA, 2 edn., 2006.

Seok, B., Helmig, D., Ganzeveld, L., Williams, M. W., and Vogel, C. S.: Dynamics of nitrogen oxides and ozone above and within a mixed hardwood forest in northern Michigan, Atmospheric Chemistry and Physics, 13, 7301–7320, https://doi.org/10.5194/acp-13-7301-2013, https://acp.copernicus.org/articles/13/7301/2013/, 2013.

Sparks, J. P., Monson, R. K., Sparks, K. L., and Lerdau, M.: Leaf uptake of nitrogen dioxide (NO2) in a tropical wet forest: implications for tropospheric chemistry, Oecologia, 127, 214–221, https://doi.org/10.1007/s004420000594, https://www.ncbi.nlm.nih.gov/pubmed/24577652, 2001.

Squizzato, S., Masiol, M., Brunelli, A., Pistollato, S., Tarabotti, E., Rampazzo, G., and Pavoni, B.: Factors determining the formation of secondary inorganic aerosol: a case study in the Po Valley (Italy), Atmospheric Chemistry and Physics, 13, 1927–1939, https://doi.org/10.5194/acp-13-1927-2013, https://acp.copernicus.org/articles/13/1927/2013/, 2013.

Stella, P., Kortner, M., Ammann, C., Foken, T., Meixner, F. X., and Trebs, I.: Measurements of nitrogen oxides and ozone fluxes by eddy covariance at a meadow: evidence for an internal leaf resistance to NO_2, Biogeosciences, 10, 5997–6017, https://doi.org/10.5194/bg-10-5997-2013, http://www.biogeosciences.net/10/5997/2013/, 2013.

Sutton, M. A., Asman, W. A. H., and Schjorring, J. K.: Dry Deposition of Reduced Nitrogen, Tellus Series B-Chemical and Physical Meteorology, 46, 255–273, https://doi.org/10.1034/j.1600-0889.1994.t01-2-00002.x, https://onlinelibrary.wiley.com/doi/abs/10.1034/j.1600-0889.1994.t01-2-00002.x, 1994.

Sutton, M. A., Schjorring, J. K., Wyers, G. P., Duyzer, J. H., Ineson, P., and Powlson, D. S.: Plant—atmosphere exchange of ammonia, Philosophical Transactions of the Royal Society of London. Series A: Physical and Engineering Sciences, 351, 261–278, https://doi.org/10.1098/rsta.1995.0033, http://rsta.royalsocietypublishing.org/cgi/doi/10.1098/rsta.1995.0033, 1995.

Sutton, M. A., Burkhardt, J. K., Guerin, D., Nemitz, E., and Fowler, D.: Development of resistance models to describe measurements of bi-directional ammonia surface–atmosphere exchange, Atmospheric Environment, 32, 473–480, https://doi.org/10.1016/s1352-2310(97)00164-7, http://www.sciencedirect.com/science/article/pii/S1352231097001647http://linkinghub.elsevier.com/retrieve/pii/S1352231097001647, 1998.

Sutton, M. A., Tang, Y. S., Miners, B., and Fowler, D.: A New Diffusion Denuder System for Long-Term, Regional Monitoring of Atmospheric Ammonia and Ammonium, Water, Air and Soil Pollution: Focus, 1, 145–156, https://doi.org/10.1023/a:1013138601753, https://doi.org/10.1023/A:1013138601753, 2001.

Sutton, M. A., Simpson, D., Levy, P. E., Smith, R. I., Reis, S., van Oijen, M., and de Vries, W.: Uncertainties in the relationship between atmospheric nitrogen deposition and forest carbon sequestration, Global Change Biology, 14, 2057–2063, https://doi.org/10.1111/j.1365-2486.2008.01636.x, https://onlinelibrary.wiley.com/doi/abs/10.1111/j.1365-2486.2008.01636.x, 2008.

Sutton, M. A., Howard, C. M., Erisman, J. W., Billen, G., Bleeker, A., Grennfelt, P., van Grinsven, H., and Grizzetti, B., eds.: The European Nitrogen Assessment: sources, effects and policy perspectives, Cambridge University Press, Cambridge, UK, 2011.

Sutton, M. A., Reis, S., Riddick, S. N., Dragosits, U., Nemitz, E., Theobald, M. R., Tang, Y. S., Braban, C. F., Vieno, M., Dore, A. J., Mitchell, R. F., Wanless, S., Daunt, F., Fowler, D., Blackall, T. D., Milford, C., Flechard, C. R., Loubet, B., Massad, R., Cellier, P., Personne, E., Coheur, P. F., Clarisse, L., Van Damme, M., Ngadi, Y., Clerbaux, C., Skjoth, C. A., Geels, C., Hertel, O., Wichink Kruit, R. J., Pinder, R. W., Bash, J. O., Walker, J. T., Simpson, D., Horvath, L., Misselbrook, T. H., Bleeker, A., Dentener, F., and de Vries, W.: Towards a climate-dependent paradigm of ammonia emission and deposition, Philosophical Transactions of the Royal Society of London. Series B.: Biological Sciences, 368, 20130 166, https://doi.org/10.1098/rstb.2013.0166, https://www.ncbi.nlm.nih.gov/pubmed/23713128, 2013.

Tang, Y. S., Simmons, I., van Dijk, N., Di Marco, C., Nemitz, E., Dämmgen, U., Gilke, K., Djuricic, V., Vidic, S., Gliha, Z., Borovecki, D., Mitosinkova, M., Hanssen, J. E., Uggerud, T. H., Sanz, M. J., Sanz, P., Chorda, J. V., Flechard, C. R., Fauvel, Y., Ferm, M., Perrino, C., and Sutton, M. A.: European scale application of atmospheric reactive nitrogen measurements in a low-cost approach to infer dry deposition fluxes, Agriculture, Ecosystems and Environment, 133, 183–195, https://doi.org/10.1016/j.agee.2009.04.027, http://www.sciencedirect.com/science/article/pii/S0167880909001388, 2009.

Tang, Y. S., Flechard, C. R., Dämmgen, U., Vidic, S., Djuricic, V., Mitosinkova, M., Uggerud, H. T., Sanz, M. J., Simmons, I., Dragosits, U., Nemitz, E., Twigg, M., van Dijk, N., Fauvel, Y., Sanz-Sanchez, F., Ferm, M., Perrino, C., Catrambone, M., Leaver, D., Braban, C. F., Cape, J. N., Heal, M. R., and Sutton, M. A.: Pan-European rural atmospheric monitoring network shows dominance of NH_3 gas and NH_4NO_3 aerosol in inorganic pollution load, Atmospheric Chemistry and Physics Discussions, 2020, 1–61, https://doi.org/10.5194/acp-2020-275, https://acp.copernicus.org/preprints/acp-2020-275/, 2020.

Tarnay, L. W., Gertler, A., and Taylor, G. E.: The use of inferential models for estimating nitric acid vapor deposition to semi-arid coniferous forests, Atmospheric Environment, 36, 3277–3287, https://doi.org/10.1016/S1352-2310(02)00303-5, http://www.sciencedirect.com/science/article/pii/S1352231002003035, 2002.

Teklemmariam, T. and Sparks, J.: Leaf fluxes of NO and NO2 in four herbaceous plant species: The role of ascorbic acid, Atmospheric Environment, 40, 2235–2244, https://doi.org/10.1016/j.atmosenv.2005.12.010, 2006.

Thoene, B., Schröder, P., Papen, H., Egger, A., and Rennenberg, H.: Absorption of atmospheric NO2 by spruce (Picea abies L. Karst.) trees, New Phytologist, 117, 575–585, https://doi.org/https://doi.org/10.1111/j.1469-8137.1991.tb00962.x, https://nph.onlinelibrary.wiley.com/doi/abs/10.1111/j.1469-8137.1991.tb00962.x, 1991.

Thoene, B., Rennenberg, H., and Weber, P.: Absorption of atmospheric NO_2 by spruce (Picea abies) trees, New Phytologist, 134, 257–266, https://doi.org/j.1469-8137.1996.tb04630.x, https://nph.onlinelibrary.wiley.com/doi/abs/10.1111/j.1469-8137.1996.tb04630.x, 1996.

UNECE: International Cooperative Program on Integrated Monitoring of Air pollution Effects on Ecosystems (ICP IM) within the framework of the Geneva Convention on Long-Range Transboundary, http://www.unece.org/env/lrtap/, last access: 17 June 2020, 2020.

Van Oss, R., Duyzer, J., and Wyers, P.: The influence of gas-to-particle conversion on measurements of ammonia exchange over forest, Atmospheric Environment, 32, 465 – 471, https://doi.org/https://doi.org/10.1016/S1352-2310(97)00280-X, http://www.sciencedirect.com/science/article/pii/S135223109700280X, 1998.

van Zanten, M. C., Sauter, F. J., Wichink Kruit, R. J., van Jaarsveld, J. A., and van Pul, W. A. J.: Description of the DEPAC module; Dry deposition modeling with DEPAC_GCN2010, Tech. rep., RIVM, Bilthoven, NL, 2010.

Vickers, D. and Mahrt, L.: Quality Control and Flux Sampling Problems for Tower and Aircraft Data, Journal of Atmospheric and Oceanic Technology, 14, 512–526, https://doi.org/10.1175/1520-0426(1997)014<0512:QCAFSP>2.0.CO;2, http://doi.org/10.1175/1520-0426(1997)014<0512:QCAFSP>2.0.CO;2, 1997.

Webb, E. K.: Profile relationships: The log-linear range, and extension to strong stability, Quarterly Journal of the Royal Meteorological Society, 96, 67–90, https://doi.org/10.1002/qj.49709640708, https://rmets.onlinelibrary.wiley.com/doi/abs/10.1002/qj.49709640708, 1970.

Wentworth, G. R., Murphy, J. G., Benedict, K. B., Bangs, E. J., and Collett Jr, J. L.: The role of dew as a nighttime reservoir and morning source for atmospheric ammonia, Atmospheric Chemistry and Physics Discussions, 16, 1–36, https://doi.org/10.5194/acp-2016-169, http://www.atmos-chem-phys-discuss.net/acp-2016-169/, 2016.

Wesely, M. L.: Parameterization of Surface Resistances to Gaseous Dry Deposition in Regional-Scale Numerical-Models, Atmospheric Environment, 23, 1293–1304, https://doi.org/Doi 10.1016/0004-6981(89)90153-4, http://www.sciencedirect.com/science/article/pii/0004698189901534, 1989.

Whitehead, J. D., Twigg, M., Famulari, D., Nemitz, E., Sutton, M. A., Gallagher, M. W., and Fowler, D.: Evaluation of laser absorption spectroscopic techniques for eddy covariance flux measurements of ammonia, Environ Sci Technol, 42, 2041–6, https://doi.org/10.1021/es071596u, https://www.ncbi.nlm.nih.gov/pubmed/18409634, 2008.

Wichink Kruit, R. J., van Pul, W. A. J., Sauter, F. J., van den Broek, M., Nemitz, E., Sutton, M. A., Krol, M., and Holtslag, A. A. M.: Modeling the surface–atmosphere exchange of ammonia, Atmospheric Environment, 44, 945–957, https://doi.org/10.1016/j.atmosenv.2009.11.049, http://www.sciencedirect.com/science/article/pii/S1352231009010346, 2010.

Wichink Kruit, R. J., Aben, J., de Vries, W., Sauter, F., van der Swaluw, E., van Zanten, M. C., and van Pul, W. A. J.: Modelling trends in ammonia in the Netherlands over the period 1990–2014, Atmospheric Environment, 154, 20–30, https://doi.org/10.1016/j.atmosenv.2017.01.031, https://www.sciencedirect.com/science/article/pii/S1352231017300316, 2017.

Wilczak, J. M., Oncley, S. P., and Stage, S. A.: Sonic Anemometer Tilt Correction Algorithms, Boundary-Layer Meteorology, 99, 127–150, https://doi.org/10.1023/A:1018966204465, https://doi.org/10.1023/A:1018966204465, 2001.

Wintjen, P., Ammann, C., Schrader, F., and Brümmer, C.: Correcting high-frequency losses of reactive nitrogen flux measurements, Atmospheric Measurement Techniques, 13, 2923–2948, https://doi.org/10.5194/amt-13-2923-2020, https://www.atmos-meas-tech.net/13/2923/2020/, 2020.

Wolff, V., Trebs, I., Foken, T., and Meixner, F. X.: Exchange of reactive nitrogen compounds: concentrations and fluxes of total ammonium and total nitrate above a spruce canopy, Biogeosciences, 7, 1729–1744, https://doi.org/10.5194/bg-7-1729-2010, https://www.biogeosciences.net/7/1729/2010/, 2010.

Wyers, G. and Duyzer, J.: Micrometeorological measurement of the dry deposition flux of sulphate and nitrate aerosols to coniferous forest, Atmospheric Environment, 31, 333 – 343, https://doi.org/https://doi.org/10.1016/S1352-2310(96)00188-4, http://www.sciencedirect.com/science/article/pii/S1352231096001884, 1997.

Wyers, G. P. and Erisman, J. W.: Ammonia exchange over coniferous forest, Atmospheric Environment, 32, 441–451, https://doi.org/10.1016/S1352-2310(97)00275-6, http://www.sciencedirect.com/science/article/pii/S1352231097002756, 1998.

Zöll, U., Brümmer, C., Schrader, F., Ammann, C., Ibrom, A., Flechard, C. R., Nelson, D. D., Zahniser, M., and Kutsch, W. L.: Surface–atmosphere exchange of ammonia over peatland using QCL-based eddy-covariance measurements and inferential modeling, Atmospheric Chemistry and Physics, 16, 11 283–11 299, https://doi.org/10.5194/acp-16-11283-2016, http://www.atmos-chem-phys.net/16/11283/2016/, 2016.

Zöll, U., Lucas-Moffat, A. M., Wintjen, P., Schrader, F., Beudert, B., and Brümmer, C.: Is the biosphere-atmosphere exchange of total reactive nitrogen above forest driven by the same factors as carbon dioxide? An analysis using artificial neural networks, Atmospheric Environment, 206, 108–118, https://doi.org/10.1016/j.atmosenv.2019.02.042, http://www.sciencedirect.com/science/article/pii/S1352231019301463, 2019.